EPJ E
Soft Matter and Biological Physics
EPJ.org
your physics journal

Eur. Phys. J. E (2015) **38**: 44 DOI 10.1140/epje/i2015-15044-1

Stochastic mechanical degradation of multi-cracked fiber bundles with elastic and viscous interactions

Fabio Manca, Stefano Giordano, Pier Luca Palla and Fabrizio Cleri

edp sciences
Società Italiana di Fisica
Springer

Eur. Phys. J. E (2015) **38**: 44
DOI 10.1140/epje/i2015-15044-1

THE EUROPEAN PHYSICAL JOURNAL E

Regular Article

Stochastic mechanical degradation of multi-cracked fiber bundles with elastic and viscous interactions

Fabio Manca[1,2], Stefano Giordano[1,2,a], Pier Luca Palla[1,3], and Fabrizio Cleri[1,3]

[1] Institute of Electronics, Microelectronics and Nanotechnology (IEMN UMR CNRS 8520), 59652 Villeneuve d'Ascq, France
[2] Joint International Laboratory LIA LEMAC/LICS, ECLille, ComUE Lille Nord de France, 59652 Villeneuve d'Ascq, France
[3] University of Lille I, 59652 Villeneuve d'Ascq, France

Received 30 January 2015 and Received in final form 20 March 2015
Published online: 25 May 2015 –

Abstract. The mechanics of fiber bundles has been largely investigated in order to understand their complex failure modes. Under a mechanical load, the fibers fail progressively while the load is redistributed among the unbroken fibers. The classical fiber bundle model captures the most important features of this rupture process. On the other hand, the homogenization techniques are able to evaluate the stiffness degradation of bulk solids with a given population of cracks. However, these approaches are inadequate to determine the effective response of a degraded bundle where breaks are induced by non-mechanical actions. Here, we propose a method to analyze the behavior of a fiber bundle, undergoing a random distribution of breaks, by considering the intrinsic response of the fibers and the visco-elastic interactions among them. We obtain analytical solutions for simple configurations, while the most general cases are studied by Monte Carlo simulations. We find that the degradation of the effective bundle stiffness can be described by two scaling regimes: a first exponential regime for a low density of breaks, followed by a power-law regime at increasingly higher break density. For both regimes, we find analytical effective expressions described by specific scaling exponents.

1 Introduction

Bundle structures are present in several natural materials and technological applications. The mechanical properties of filamentous biopolymers, such as cytoskeletal proteins, f-actin and microtubules, play a crucial role in several processes of eukaryotic cells [1]. Also at a larger scale-length, fiber bundles are ordinarily occurring biomaterials: one can mention collagen, spider silk, bone, tendon, and skin, which are structures exhibiting the rare combination of large strength and high toughness [2–7]. These materials make use of important geometrical and physical features like the hierarchical assemblage [8], the twisted geometry [9], the optimized equilibrium between defects and width [10], and the beneficial disorder increasing the overall strength [11]. On the other hand, the mechanical performance of artificial materials increases progressively with the development of technology. As an example, carbon nanotube (CNT) assemblies have been produced with different geometries, such as one-dimensional CNT fibers [12], two-dimensional CNT films/sheets [13], and three-dimensional aligned CNT arrays [14]. These macroarchitectures exhibit several interesting properties, which depend on the adopted technological fabrication procedure [15]. For instance, the embedding of CNT fibers in polymer matrices allow to obtain composite materials with excellent strength and stiffness [16]. Moreover, CNT-based macroscopic cables with different lengths and microstructures have been envisaged and several multiscale stochastic simulations have been carried out to test their tensile response and to optimize their design [17].

Since its paradigmatic importance, the fiber bundle geometry gained consideration over the years to study failure, rupture, creep and fatigue phenomena caused by cascades in model materials [18,19]. The so-called fiber bundle model (FBM) was introduced for studying the failure of spun cotton yarns [20], and it was further elaborated by Daniels [21] for considering a parallel arrangement of fibers with statistically distributed strength (stress threshold before rupture). Within this model, when an external load produces the failure of a fiber, its fraction of load is equally distributed among the intact fibers: this is the so-called global load sharing (GLS) rule [21]. Another redistribution strategy is the local load sharing (LLS) rule, assuming that the load of a broken fiber is carried only by the nearest intact fibers [22]. This sharing rule allows to develop different solvable models [23–25]. We remark that the GLS and the LLS rules belong to distinct universality classes [26–30]. Other approaches have been proposed to describe

[a] e-mail: Stefano.Giordano@iemn.univ-lille1.fr

different properties and phenomena, such as the visco-elasticity [31], the power-law creep compliance [32–34], the plasticity [35,36], the continuous damage [37,38], the effects of the strain gradient [39], and the result of discontinuities in the threshold distribution [40]. More recently, also the relaxation times [41], the brittle-to-ductile transition [42], and the constrained crack growth [43] have been investigated in the context of the FBM.

While the FBM and its modifications are useful to describe the failure as accumulation of localized breaks, generated by the application of an external mechanical load, the classical homogenization techniques are more appropriate to determine the effective stiffness of a structure degraded by a given population of breaks [44–46]. In the first case the distribution of breaks is a result of the model solution, while in the second one it is the input leading to the effective response. From the historical point of view, classical results in homogenization theory concern the existence of upper and lower bounds for the effective elastic moduli of composite materials [47,48] and expressions based on the spatial correlation among the constituents [49,50]. As a matter of fact, one of the most studied homogenization theories is addressed to a dilute dispersion of spherical [44,45] or ellipsoidal [51] inhomogeneities embedded in a solid matrix. These results have been generalized to consider higher concentrations of inhomogeneities through the iterated homogenization technique [52] and the differential effective medium theory [53,54]. The central point of these methods is the Eshelby theory, concerning the elastic behavior of a single ellipsoidal inhomogeneity embedded in a different matrix [55]. We remark that a fracture is typically considered as a void ellipsoid of vanishing eccentricity: this technique allows to develop efficient effective medium theories for multi-cracked materials [56,57]. Recent results concern the effects of the orientational distribution of cracks [58,59], the effects of the anisotropy [60], and computational methods [61].

Although the fiber bundle structure has been considered within the FBM context, this geometry has not been investigated through homogenization techniques, which are typically applied to bulk solid materials. The present investigation is therefore addressed to understand the mechanical properties of a degraded fiber bundle by means of the homogenization approach. This point is especially important when breaks are not caused by a mechanical load, but rather by an external action (*e.g.* chemical, thermal, or electromagnetic). As prominent examples, we may cite the degradation induced by some antibiotics in tendon collagen [62], the lysis of muscle sarcomeres produced by some statins [63], the damage in the form of single- and double-strand breaks in DNA irradiated by high-energy photons [64–66], or degraded by restriction enzymes [67,68]. At more macroscopic scales, examples include corrosion of high-voltage power cable bundles [69], suspended-bridge steel cables [70], or meshes in concrete structures [71], loss of cohesion in tree-root bundles with variable soil wetness, triggering shallow landslides [72,73].

In this work, we introduce a physical model of an interacting fiber bundle, together with a procedure able to determine the mechanical effective properties of set of M fibers degraded by means of a distribution of N breaks. This general scheme represents most features of the above-cited examples. In our previous work we introduced the study of the purely elastic case [74]. Here, we develop a more complete homogenization scheme, able to take into consideration both the intrinsic visco-elasticity of the fibers and the possible visco-elastic interactions among them as mediated by a surrounding matrix. From the geometrical point of view, although the general scheme is able to deal with arbitrary arrangements, the examples developed will concern flat and circular geometries (see fig. 1). We remark that the origin of the stochastic process in our scheme is limited to the random generation of breaks within the bundle assembly. Indeed, we study the purely mechanical response without considering the temperature effects, which are classically described by the statistical mechanics formalism [75]. The thermo-elasticity of polymeric structures have been largely studied but limited to the response of a single chain [76–79].

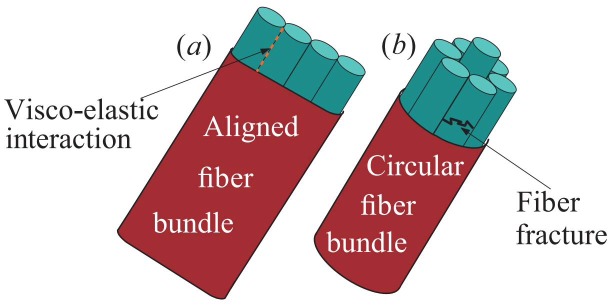

Fig. 1. Schemes of two different geometries of a fiber bundle with flat (a) and circular (b) shape.

The structure of the paper is the following. In sect. 2 we present the formalism for analysing the mechanics of the fiber bundle with and without a population of breaks. As a result we obtain an exact homogenization scheme, which can be easily implemented in a software code. In sect. 3 we present some analytical results useful to frame the successive numerical achievements in a well-defined picture. More specifically, we consider a first simple bundle composed of just two interacting fibers and a second case concerning M non-interacting fibers with a population of N randomly distributed breaks. For both cases, we obtain closed-form expressions for the effective stiffness of the bundle, which contain almost all the features that can be observed in more complex systems. In sect. 4 we present the numerical results for arbitrary complex fiber and break arrangements and their physical interpretations. In particular, we show that the degradation of the bundle response is always nearly exponential for a low number of breaks and it shows a shift towards a power-low behavior for a larger number. We analyse the scaling behavior of these two different regimes and we obtain the corresponding asymptotic expressions described by specific scaling exponents. At the end of sect. 4, numerical results and their interpretations are presented for both elastic and viscous interactions among the fibers.

2 Modelling the fiber bundle

We introduce here the mathematical description of the fiber bundle mechanics: we start with an intact bundle, and then we subsequently analyze a bundle with an arbitrary population of breaks.

2.1 Formalism for the intact bundle

To begin, we take into consideration a single elastic fiber, with circular cross-section of area S, and length l. The longitudinal deformation of this one-dimensional system is described by the scalar stress $T(x,t)$, where x is the linear abscissa along the fiber ($0 < x < l$) and t is the time. If we consider a small fiber segment of length $\mathrm{d}x$ located at x, we can write the balance of forces as $F(x,t) + G(x,t)S\mathrm{d}x = \rho S\mathrm{d}x a(x,t)$, where $F(x,t) = T(x+\mathrm{d}x,t)S - T(x,t)S$ is the force applied by the remaining parts of the fiber (on the left and on the right), $G(x,t)$ is the externally applied body force (per unit of volume), ρ is the mass density, and a is the acceleration of the segment of fiber itself. Of course, we have $a(x,t) = \partial^2 U(x,t)/\partial t^2$, where $U(x,t)$ is the longitudinal displacement along the fiber. It means that, during the deformation, the point originally located at x, assumes the position $x+U(x,t)$ at time t. By dividing the above balance equation by $S\mathrm{d}x$ and performing the limit for $\mathrm{d}x \to 0$, we obtain the equation

$$\frac{\partial T(x,t)}{\partial x} + G(x,t) = \rho \frac{\partial^2 U(x,t)}{\partial t^2}. \tag{1}$$

Moreover, we have to introduce the constitutive equation for the elasticity of the fiber. To do this, we consider a linear relationship (Hooke law) between the stress and the deformation, defined as $\epsilon(x,t) = \partial U(x,t)/\partial x$

$$T(x,t) = E\epsilon(x,t) = E\frac{\partial U(x,t)}{\partial x}, \tag{2}$$

where E is the Young modulus of the fiber. By combining eqs. (1) and (2) one obtains the classical one-dimensional wave equation for the displacement $U(x,t)$. However, it is convenient, for the development of our model, to preserve the two-variable (T and U) approach, thus based on two coupled equations.

Let us now consider a bundle of M fibers, which are parallel but arbitrarily arranged on the perpendicular plane (cross-section of the bundle). For instance, we may consider a bundle of fibers aligned on a given plane, as in fig. 1a, or regularly packed on a triangular lattice (with hexagonal symmetry), as in fig. 1b. Each fiber is coupled with other fibers of the bundle by means of a visco-elastic interaction. Therefore, the system is described by the following set of equations:

$$\frac{\partial T_i(x,t)}{\partial x} = -G_i(x,t) + \rho_i \frac{\partial^2 U_i(x,t)}{\partial t^2}, \tag{3}$$

$$\frac{\partial U_i(x,t)}{\partial x} = \frac{1}{E_i} T_i(x,t), \tag{4}$$

for $\forall i = 1, \ldots, M$, where

$$G_i(x,t) = \sum_{j=1}^{M} \left(k_{ij} + h_{ij}\frac{\partial}{\partial t} \right)(U_j - U_i). \tag{5}$$

Here, the coefficients k_{ij} represent the elastic coupling and the h_{ij} the viscous one. The symmetrical matrices k_{ij} and h_{ij} (with $k_{ii} = 0$ and $h_{ii} = 0$) are straightforwardly associated to the graph describing the fiber interactions on the cross-section of the bundle.

In order to simplify the analysis of the system we assume a sinusoidal time dependence of all mechanical quantities. In so doing, the partial differential equations are transformed into simpler ordinary differential equations. We recall that an arbitrary function $\Psi(x,t)$, in a given sinusoidal stationary regime (at frequency ω), can be written in the phasor form $\Psi(x,t) = \mathfrak{Re}\{\psi(x)e^{i\omega t}\}$, where $\psi(x)$ is a given complex function. Under these conditions, we have the standard correspondence $\Psi(x,t) \to \psi(x)$, $\partial\Psi(x,t)/\partial t \to i\omega\psi(x)$, and $\partial\Psi(x,t)/\partial x \to \mathrm{d}\psi(x)/\mathrm{d}x$. Consequently, the equations of the bundle can be simplified as follows:

$$\frac{\mathrm{d}t_i(x)}{\mathrm{d}x} = -g_i(x) - \rho_i\omega^2 u_i(x), \tag{6}$$

$$\frac{\mathrm{d}u_i(x)}{\mathrm{d}x} = \frac{1}{E_i} t_i(x), \tag{7}$$

where

$$g_i(x) = \sum_{j=1}^{M} (k_{ij} + i\omega h_{ij})(u_j - u_i). \tag{8}$$

We observe that the capital letters (real physical quantities) have been substituted with the corresponding complex phasors (here indicated with lower-case letters). The introduction of the viscous interactions can be therefore done by considering a frequency-dependent complex coefficient $k_{ij} + i\omega h_{ij}$ in place of k_{ij}, used for the purely elastic case [74]. Also, E_i can be considered as a complex parameter, by introducing the intrinsic viscosity of each fiber.

Defining $\boldsymbol{\xi}$ ($\in \mathbb{C}^{2M}$) as the vector containing all the variables (t_1, u_1, t_2, u_2, …, t_M, u_M), the system of equations can be easily written in the compact form

$$\frac{\mathrm{d}\boldsymbol{\xi}}{\mathrm{d}x} = \mathbf{A}\boldsymbol{\xi}. \tag{9}$$

where $\mathbf{A}$ is a $2M \times 2M$ constant complex matrix, depending on E_i, ρ_i, k_{ij} and h_{ij} for any $i, j = 1 \ldots M$. Therefore, the dynamics of the intact system (without breaks) can be simply studied by means of the matrix exponential $\exp(\mathbf{A}x)$. The pertinent boundary conditions will be discussed in the next section, where we also introduce a method to deal with a given population of breaks distributed among the fibers.

2.2 Bundle description with an arbitrary distribution of breaks

We now consider the fiber bundle above with a population of breaks arbitrarily distributed within the structure.

More precisely, we suppose to deal with N breaks located at positions x_i, $i = 1, \ldots, N$. We also assume that the break located at x_i is applied to the j_i-th fiber of the bundle (it means that $j_i \in \{1, 2, \ldots, M\}$, $\forall i = 1, \ldots, N$). We define for convenience $x_0 = 0$ (left end-terminal of the bundle) and $x_{N+1} = l$ (right end-terminal of the bundle). It is important to remark that, when a fiber is broken in one or more points, it continues to contribute to the overall stiffness of the bundle through the lateral interactions with the other fibers, controlled by the elastic coefficients k_{ij} and the viscous ones h_{ij}. This means that the structure of the bundle remains unchanged also with the introduction of the breaks population. If N breaks are distributed on the structure, this defines $N+1$ intact segments in the entire bundle identified by $x \in (x_i, x_{i+1})$, $\forall i = 0, \ldots, N$. Hence, for each of the above segments we can write

$$\boldsymbol{\xi}(x_{i+1}^-) = \exp\left[\mathbf{A}(x_{i+1} - x_i)\right] \boldsymbol{\xi}(x_i^+), \tag{10}$$

where $\boldsymbol{\xi}(x)$ is the vector defined in eq. (9). Moreover, we adopted the notation $\boldsymbol{\xi}(x_i^\pm) = \lim_{x \to x_i^\pm} \boldsymbol{\xi}(x)$: x_i^+ means that x_i is approached from the right and, similarly, x_i^- means that x_i is approached from the left. It is important to distinguish between the left- and right-hand limits since the presence of breaks causes the lack of continuity of some elastic quantities. Therefore, the quantities $\boldsymbol{\xi}(x_0)$, $\boldsymbol{\xi}(x_1^-)$, $\boldsymbol{\xi}(x_1^+)$, $\boldsymbol{\xi}(x_2^-)$, $\ldots$, $\boldsymbol{\xi}(x_{N-1}^+)$, $\boldsymbol{\xi}(x_N^-)$, $\boldsymbol{\xi}(x_N^+)$, $\boldsymbol{\xi}(x_{N+1})$ will be considered independent unknowns in the following development. In order to mimic the breaks, we must consider the following boundary conditions for $x = x_i$ ($i = 1, \ldots, N$):

$$u_k(x_i^-) = u_k(x_i^+), \quad \forall k = 1, \ldots, M, k \neq j_i, \tag{11}$$

$$t_k(x_i^-) = t_k(x_i^+), \quad \forall k = 1, \ldots, M, k \neq j_i, \tag{12}$$

$$t_{j_i}(x_i^-) = 0 \quad \text{and} \quad t_{j_i}(x_i^+) = 0. \tag{13}$$

Equations (11) e (12) represent the continuity of the longitudinal displacement and stress in the intact fibers ($k \neq j_i$). On the other hand, eq. (13) means that there is no transmission of force across the broken fiber ($k = j_i$). In this case, the displacement shows an unknown jump, which can be determined by the application of the present procedure. Moreover, we consider a given displacement prescribed to the right end of the bundle ($x = l$), while the head of the bundle ($x = 0$) is kept fixed

$$u_k(x_0) = u_k(0) = 0, \quad \forall k = 1, \ldots, M, \tag{14}$$

$$u_k(x_{N+1}) = u_k(l) = \delta, \quad \forall k = 1, \ldots, M, \tag{15}$$

where δ is a real parameter. It is important to observe that the last condition, translated to the real physical quantities, reads $U_k(l,t) = \delta \cos(\omega t)$, representing an imposed oscillating displacement at the right end-terminal of the bundle. This dynamic forcing term is important to investigate the effective visco-elastic behavior of the fiber bundle, introduced in eq. (8).

We prove now that all conditions summarized are necessary and sufficient to solve the problem with M fibers and N breaks. All the unknowns can be grouped in the following vector:

$$\boldsymbol{\eta} = \begin{bmatrix} \boldsymbol{\xi}(x_0) \\ \boldsymbol{\xi}(x_1^-) \\ \boldsymbol{\xi}(x_1^+) \\ \boldsymbol{\xi}(x_2^-) \\ \cdots \\ \boldsymbol{\xi}(x_{N-1}^+) \\ \boldsymbol{\xi}(x_N^-) \\ \boldsymbol{\xi}(x_N^+) \\ \boldsymbol{\xi}(x_{N+1}) \end{bmatrix}, \tag{16}$$

which contains $2(N+1)$ sub-vectors, each of them having $2M$ complex components. As a consequence, we have a total number of $4M(N+1)$ unknowns (equivalently, $\boldsymbol{\eta} \in \mathbb{C}^{4M(N+1)}$). The available equations can be counted as follows. The $N+1$ vector relationships given in eqs. (10) ($i = 0, \ldots, N$) correspond to $2M(N+1)$ scalar equations. Moreover, the break conditions given in eqs. (11), (12) and (13) correspond to $2MN$ relations. Finally, the boundary conditions summed up in eqs. (14) and (15) stand for $2M$ equalities. To conclude, we observe that $2M(N+1) + 2MN + 2M = 4M(N+1)$, proving the possibility to solve the problem by means of a system of equations, which can be written as

$$\mathbf{B}\boldsymbol{\eta} = \boldsymbol{b}. \tag{17}$$

Here, $\mathbf{B}$ is a non-singular $4M(N+1)$ by $4M(N+1)$ matrix representing all the conditions stated in eqs. (10), (11), (12), (13), (14) and (15), and $\boldsymbol{b} \in \mathbb{C}^{4M(N+1)}$ is a vector directly depending on the prescribed displacement δ. We note that, from the computational point of view, the construction of the matrix $\mathbf{B}$ is rather onerous since it is composed, among other simpler sub-matrices, of $N+1$ matrix exponentials of size $2M \times 2M$. We developed an efficient software code to solve the problem for an arbitrary bundle with M fibers and N breaks. While the algorithm for the matrix exponential has been based on the rational Padé approximants, the solution of eq. (17) has been approached with standard techniques for sparse matrices. Hence, for a given distribution of breaks we can determine the effective elastic response of the overall bundle as follows: by solving eq. (17) we obtain the stresses on the right end-terminals of the fibers $t_k(x_{n+1}) = t_k(l)$ ($\forall k = 1, \ldots, M$); the total stress $\sum_{i=1}^{M} t_k(l)$ can be divided by the overall strain δ/l, to obtain the effective complex stiffness

$$E_{\text{eff}} = \frac{l}{\delta} \sum_{i=1}^{M} t_k(l). \tag{18}$$

This represents the complex Young modulus of a single effective fiber, which is equivalent to the whole bundle with M fibers and N breaks. Of course, the actual value of E_{eff} depends on the frequency ω, and it can be seen as a transfer function, useful to perform the spectral analysis of the system.

It is interesting to observe that this computational scheme can be used to determine the effects of a random distribution of breaks within the bundle. In fact, we can apply the Monte Carlo method by considering several structures with randomly chosen breaks distribution and by calculating the pertinent average values. We will use this approach in the following section 4.

3 Analytical results

In order to better understand the general behavior of the bundle model introduced above, we consider two particular cases that can be studied by means of analytical techniques.

The first case deals with a simple bundle composed of two interacting fibers. We investigate the effects of a geometrically regular distribution of breaks on this structure. The results can be applied to the case of purely elastic, purely viscous or visco-elastic interactions.

The second case concerns a bundle composed of M non-interacting fibers with a population of N randomly distributed breaks. By means of a probabilistic approach, we can analyse the stochastic mechanical degradation of this system.

In both cases we obtain closed-form expressions for the effective stiffness of the bundle. These results are useful to check the general computational scheme discussed in the previous section. Moreover, they contain almost all the features that can be observed in more complex systems. The combination of the random character of the breaks distribution with an arbitrary interaction among $M > 2$ fibers will be investigated in the next section through Monte Carlo simulations.

3.1 The multi-cracked bundle with two elastically interacting fibers

To begin, we take into consideration a couple of interacting fibers in static regime, *i.e.* a simple elastic system without viscous contribution. In these conditions, the equations for an intact segment of bundle read

$$\frac{\mathrm{d}t_1(x)}{\mathrm{d}x} = k[u_1(x) - u_2(x)], \tag{19}$$

$$\frac{\mathrm{d}u_1(x)}{\mathrm{d}x} = \frac{t_1(x)}{E_1}, \tag{20}$$

$$\frac{\mathrm{d}t_2(x)}{\mathrm{d}x} = k[u_2(x) - u_1(x)], \tag{21}$$

$$\frac{\mathrm{d}u_2(x)}{\mathrm{d}x} = \frac{t_2(x)}{E_2}, \tag{22}$$

where $k = k_{12} = k_{21}$. This system can be converted into a single, fourth-order differential equation for the displacement u_1, *i.e.*

$$\frac{\mathrm{d}^4u_1(x)}{\mathrm{d}x^4} - \lambda\frac{\mathrm{d}^2u_1(x)}{\mathrm{d}x^2} = 0, \tag{23}$$

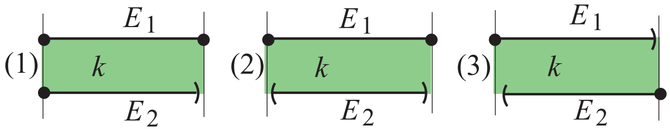

Fig. 2. Schemes of three different simple configurations of a two-fiber bundle with stiffness E_1 and E_2. The fibers are embedded in an elastic medium generating an interaction coefficient k.

where $\lambda = \sqrt{k(1/E_1 + 1/E_2)}$. So, the general solutions for u_1 and u_2 can be obtained as follows:

$$u_1(x) = c_1 + c_2x + c_3e^{-\lambda x} + c_4e^{\lambda x}, \tag{24}$$

$$u_2(x) = c_1 + c_2x - c_3\frac{E_1}{E_2}e^{-\lambda x} - c_4\frac{E_1}{E_2}e^{\lambda x}, \tag{25}$$

where c_1, c_2, c_3 and c_4 are arbitrary coefficients to be determined through the pertinent boundary conditions.

As an elementary example, we can consider the bundle composed of two intact fibers of length l. In this case the boundary conditions given in eqs. (14) and (15) simply read $u_1(0) = 0$, $u_2(0) = 0$, $u_1(l) = \delta$ and $u_2(l) = \delta$. A straightforward calculation immediately leads to the linear displacements $u_1(x) = u_2(x) = \delta x/l$. This corresponds to $E_{\text{eff}} = E_1+E_2$, meaning that the unbroken bundle behaves as an ensemble of independent and non-interacting fibers. Indeed, the effective stiffness is simply given by the sum of the individual fiber contributions.

The behavior is different and more complex if we introduce some breaks. We consider three basic configurations (see fig. 2), which are useful for the following developments:

- 1) the first fiber is intact and the second one is broken in correspondence to the right end-terminal; the boundary conditions are therefore $u_1(0) = 0$, $u_2(0) = 0$, $u_1(l) = \delta$ and $t_2(l) = 0$;
- 2) the first fiber is intact and the second one is broken in correspondence to both the left and right end-terminals; the boundary conditions are now $u_1(0) = 0$, $t_2(0) = 0$, $u_1(l) = \delta$ and $t_2(l) = 0$;
- 3) the first fiber is broken at $x = l$ while the second one at $x = 0$; in this case the boundary conditions are $u_1(0) = 0$, $t_2(0) = 0$, $t_1(l) = 0$ and $u_2(l) = \delta$.

For each configuration the exact displacements u_1 and u_2 and the effective stiffness can be easily determined. In all cases the effective stiffness is strongly influenced by the interaction coefficient k or, equivalently, by the parameter λl, as indicated in table 1. This dependence underlines the scale effects exhibited by the overall stiffness of the bundle: in very long bundles ($l \gg 1/\lambda$) the effects of the interactions are stronger and, on the contrary, in shorter bundles ($l \ll 1/\lambda$) these effects are negligible. For this reason, the quantity $1/\lambda$ may be named *two-fiber coupling length* since it modulates the length-scale effects in this system.

These results can be combined to analyse more general two-fiber multi-cracked systems. In fact, if we consider a sequence of adjacent bundle segments, each one

Table 1. Effective stiffness expressions corresponding to the three configurations introduced in fig. 2. We used the definition $\lambda = \sqrt{k(1/E_1 + 1/E_2)}$, as discussed in the main text.

Geometry	Effective stiffness
1)	$E_{\rm eff}^{1)} = \dfrac{E_1+E_2}{1+\frac{E_2}{E_1}\frac{\tanh(\lambda l)}{\lambda l}}$
2)	$E_{\rm eff}^{2)} = \dfrac{E_1+E_2}{1+2\frac{E_2}{E_1}\frac{\cosh(\lambda l)-1}{\lambda l \sinh(\lambda l)}}$
3)	$E_{\rm eff}^{3)} = \dfrac{E_1+E_2}{1+\frac{2}{\lambda l\sinh(\lambda l)}+\left(\frac{E_1}{E_2}+\frac{E_2}{E_1}\right)\frac{\coth(\lambda l)}{\lambda l}}$

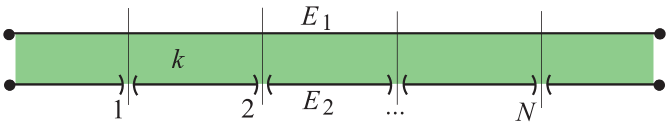

Fig. 3. Scheme of a cracked two-fiber bundle of total length l. All the N breaks (discontinuities) are localized in the second fiber.

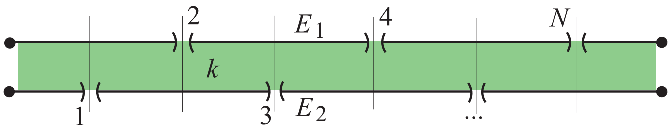

Fig. 4. Scheme of a cracked two-fiber bundle of total length l. There are N breaks alternately localized in each fiber.

corresponding to one of the models 1), 2) or 3) above, we can obtain the overall stiffness through the simple mixing law $E_{\rm eff} = l/\sum_i(l_i/E_i)$. Here, l_i is the length of the i-th segment, E_i is its stiffness and $l = \sum_i l_i$. Of course, this expression is valid only for a two-fiber bundle since there is a single contact point between every couple of adjacent segments. We consider now two multi-cracked bundle structures of total length l with the following regular distributions of breaks:

a) the first fiber is intact (without breaks) and the second one is degraded by N equispaced breaks, as represented in fig. 3; it follows that we have a sequence of $N+1$ segments, of which 2 of the type 1) (the first and the last), and $N-1$ (the central ones) of the type 2);
b) N breaks are alternately distributed in each fiber (N is an even integer), as represented in fig. 4; we have therefore a sequence of $N+1$ segments, of which 2 of the type 1) (the first and the last), and $N-1$ of the type 3);

By using the previously described mixing law $E_{\rm eff} = l/\sum_i(l_i/E_i)$, we obtain the following effective stiffness ($N \geq 1$) for the case a):

$$E_{\rm eff}^{a)}(N) = \frac{E_1+E_2}{1+2\frac{E_2}{E_1}\left[f_N(\lambda l) - g_N(\lambda l)\right]}, \tag{26}$$

and the following one for the case b)

$$E_{\rm eff}^{b)}(N) = \frac{E_1+E_2}{1+\left(\frac{E_1}{E_2}+\frac{E_2}{E_1}\right)f_N(\lambda l) + 2g_N(\lambda l)}, \tag{27}$$

where, to compact the notation, we have introduced the two functions

$$f_N(z) = \frac{1}{z}\left[\tanh\left(\frac{z}{N+1}\right) + (N-1)\coth\left(\frac{z}{N+1}\right)\right],$$
$$g_N(z) = \frac{N-1}{z}\,\mathrm{csch}\left(\frac{z}{N+1}\right). \tag{28}$$

We observe that, for N approaching infinity, $E_{\rm eff}^{a)}(N)$ converges to E_1, since the effects of the second fiber progressively vanish, and $E_{\rm eff}^{b)}(N)$ converges to zero, since both fibers are asymptotically completely degraded.

If we consider the case with $E_1 = E_2 = E$, then we obtain the simpler results

$$E_{\rm eff}^{a),b)}(N) = \frac{2E}{1+2\left[f_N\left(l\sqrt{\frac{2k}{E}}\right) \mp g_N\left(l\sqrt{\frac{2k}{E}}\right)\right]}, \tag{29}$$

where the $-$ and the $+$ signs correspond to a) and b), respectively. In fig. 5 we show the behavior of $E_{\rm eff}^{a)}(N)$ and $E_{\rm eff}^{b)}(N)$ *versus* the number N of fiber breaks, for different values of the dimensionless parameter kl^2/E.

It is interesting to study the asymptotic behavior of eq. (29) for $N \to \infty$. We obtain the expansions

$$E_{\rm eff}^{a)}(N) = E + \frac{1}{12}\frac{kl^2}{N^2} + \frac{1}{3}\frac{kl^2}{N^3} - \frac{5}{4}\frac{kl^2}{N^4} - \frac{7}{720}\frac{k^2l^4}{EN^4} + O\left(N^{-5}\right) \tag{30}$$

for the case a), and

$$E_{\rm eff}^{b)}(N) = \frac{kl^2}{N^2} + \frac{kl^2}{N^4} - \frac{2}{3}\frac{k^2l^4}{EN^4} + O\left(N^{-5}\right) \tag{31}$$

for the case b). These developments reveal a power-law dependence for large values of N, respectively

$$\lim_{N\to\infty}\frac{E_{\rm eff}^{a)}(N) - E}{\frac{kl^2}{12N^2}} = 1, \tag{32}$$
$$\lim_{N\to\infty}\frac{E_{\rm eff}^{b)}(N)}{\frac{kl^2}{N^2}} = 1, \tag{33}$$

exhibiting a degradation behavior (decrease of $E_{\rm eff}$) evolving as fast as $1/N^2$.

This simple power-law response can be easily interpreted with the following argument. If we consider the case b), we can subdivide the whole dimer in N segments with length $\Delta x = l/N$ and shear coefficient k. Therefore, for each segment we can write from eqs. (19) and (21) $\Delta t/\Delta x = k\Delta u$. Being $\Delta t = F/S$, where F is the force and S the fiber section, we can obtain $F = (Slk/N)\Delta u$.

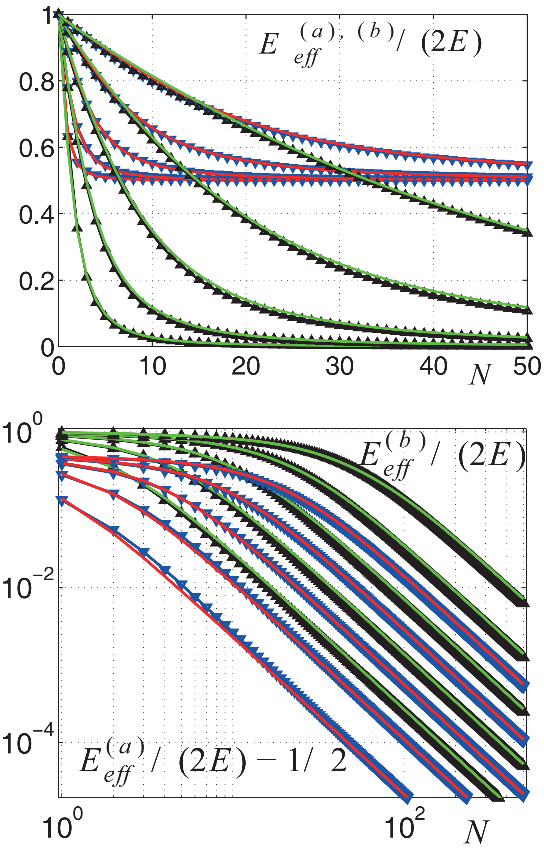

Fig. 5. Behavior of the purely elastic two-fiber bundle: effective stiffness *versus* the number of breaks (the first panel corresponds to linear scales and the second one to bi-logarithmic scales). The blue down triangles represents $E_{\text{eff}}^{\text{a)}}(N)$, while the black up triangles the stiffness $E_{\text{eff}}^{\text{b)}}(N)$ (see eq. (29)). Moreover, the continuous red and green curves correspond to the approximations given in eqs. (34) and (35). The different curves have been obtained with five different values of $z=\lambda l = l\sqrt{2k/E}$, corresponding to $kl^2/E = 5^n$, where $n=1,\dots,5$.

Hence, we identify the equivalent spring constant of each segment $K_s = Slk/N$. The effective spring constant of the dimer is then given by $K_{\text{eff}} = 1/(N/K_s) = klS/N^2$. In terms of the Young modulus we can finally write the effective response as $E_{\text{eff}}^{\text{b)}} = (l/S)K_{\text{eff}} = kl^2/N^2$, coherently with eqs. (31) and (33). This represents a simple explanation of the asymptotic behavior of the multi-cracked dimer.

This behavior is confirmed in the second panel of fig. 5, where the effective stiffness for the cases a) and b) is represented in bi-logarithmic scales. Moreover, it is important to remark that, for large N, the bundle stiffness reduction is not influenced by the Young modulus E of the fibers, as deduced from eqs. (32) and (33). The physical meaning is that, for large N, the longitudinal deformations of the fiber fragments are not important to define the overall stiffness, being relevant only the interactions, modulated by k, among the adjacent broken fibers. Therefore, after a first regime of degradation (low values of N), there is a transition to a power-law regime, describing the loss of importance of the Young modulus E, and the increase of significance of the interaction coefficient k. This transition can be efficiently represented by means of the following approximated expressions, which accurately reproduce the behavior of eq. (29):

$$\frac{E_{\text{eff}}^{\text{a)}}(N)}{2E} = \frac{1}{2} + \frac{1}{2}\frac{1}{1+4\frac{N}{z} - 6\left(\frac{N}{z}\right)^{\frac{3}{2}} + 24\left(\frac{N}{z}\right)^2}\,, \tag{34}$$

$$\frac{E_{\text{eff}}^{\text{b)}}(N)}{2E} = \frac{1}{1+2\frac{N}{z} - 2\left(\frac{N}{z}\right)^{\frac{3}{2}} + 4\left(\frac{N}{z}\right)^2}\,. \tag{35}$$

Here $z=\lambda l = l\sqrt{2k/E}$, as before. For large N, only the terms of second degree are relevant, and we obtain the above power-laws, describing the degradation of the bundle stiffness for large values of N. On the other hand, the initial slope of the degradation (for small N) is governed by the first order binomials $1+4z/N$ and $1+2z/N$, for the case a) and b), respectively. Further, the irrational terms with power $3/2$ have been introduced only to obtain a smooth connection between the two regimes, for low and high values of N. Although eqs. (34) and (35) are approximated and heuristic results, they are interesting because they directly show the physics underlying the bundle mechanical degradation. In addition, we remark that these approximated results are not essential in this context with two fibers because we know the exact solutions given in eq. (29); nevertheless, this approach of developing physically educated fittings will be very useful to interpret and understand the numerical results of next Sections. To conclude, we underline that the exact analytical results given in eq. (29) have been also accurately confirmed by the application of the general computational scheme outlined in sect. 2.2, here applied to the present structures.

3.1.1 An example of viscous interaction

We consider here an example in which, instead of purely elastic, viscous interactions exist among the fibers. In particular, we take into account the geometrical configuration b) of the previous sect. 3.1, see fig. 4. However, since only viscous interactions are introduced, the real constant k must be replaced by the purely imaginary quantity $i\omega h$, as discussed in sect. 2.1. It is also important to note that the visco-elastic bundle must be characterized by a very low mass density of the fibers in order to neglect the inertial terms in eq. (6).

It is interesting to analyse the behavior for large values of N because there are some important differences with respect to the previous, purely elastic case. Of course, eq. (29), with the sign + corresponding to the configuration b), and eq. (31) remain valid also for complex values of k. Since $E_{\text{eff}}^{\text{b)}}(N)$ is now a complex number, eq. (31) can be elaborated to obtain its real and imaginary parts, as follows:

$$\mathfrak{Re}\left\{\frac{E_{\text{eff}}^{\text{b)}}(N)}{2E}\right\} \underset{N\to\infty}{\sim} \frac{\omega^2 h^2 l^4}{3E^2N^4}\,, \tag{36}$$

$$\mathfrak{Im}\left\{\frac{E_{\text{eff}}^{\text{b})}(N)}{2E}\right\}\underset{N\to\infty}{\sim}\frac{\omega h l^2}{2EN^2}\,, \tag{37}$$

showing that the real and the imaginary parts decrease as $1/N^4$ and $1/N^2$, for large N, respectively. Therefore, we have two different scaling behaviors for the two components of the effective complex stiffness, in the case of purely viscous interactions. In particular, the simple fitting given in eq. (35) is no longer valid since it does not take into account any power of order four in its denominator. On the other hand, the behavior for small values of N is always well approximated by the relation $E_{\text{eff}}^{\text{b})}(N)/(2E) = 1/(1+2N/z)$, where $z = l\sqrt{2i\omega h/E}$. By separating the real and imaginary parts, we find

$$\mathfrak{Re}\left\{\frac{E_{\text{eff}}^{\text{b})}(N)}{2E}\right\}\underset{N\to 0}{\sim}\frac{1+\frac{N}{l\sqrt{\frac{\omega h}{E}}}}{1+\frac{2N}{l\sqrt{\frac{\omega h}{E}}}+\frac{2N^2}{l^2\frac{\omega h}{E}}}\,, \tag{38}$$

$$\mathfrak{Im}\left\{\frac{E_{\text{eff}}^{\text{b})}(N)}{2E}\right\}\underset{N\to 0}{\sim}\frac{\frac{N}{l\sqrt{\frac{\omega h}{E}}}}{1+\frac{2N}{l\sqrt{\frac{\omega h}{E}}}+\frac{2N^2}{l^2\frac{\omega h}{E}}}\,. \tag{39}$$

In figs. 6 and 7 we show an example of viscous response for different values of the quantity ωh. We plotted in red the behavior for small values of N given in eqs. (38) and (39) and, in green, the asymptotic trends defined in eqs. (36) and (37). We remark that, in this case, it is difficult to give simple expressions describing a good link between the two observed regimes. This point can be explained by observing that the imaginary part of the effective stiffness exhibits a peak, which is not represented by any of the approximated laws, for both low and high values on N. A similar behavior will be described for a bundle of $M > 2$ fibers with population of random breaks (see sect. 4.4).

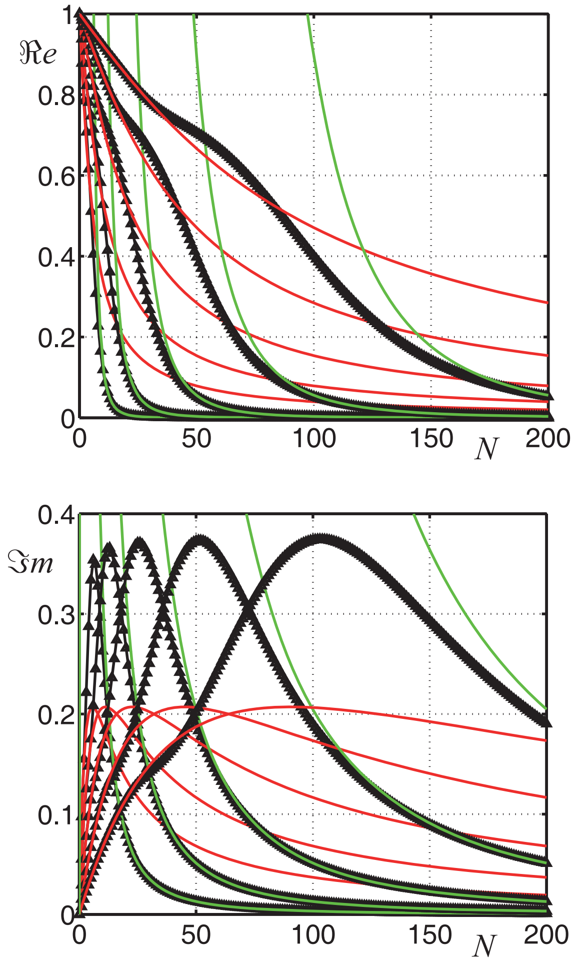

Fig. 6. Behavior of the viscous two-fiber bundle: effective stiffness (real and imaginary parts) *versus* the number of breaks. The black triangles represent the exact stiffness $E_{\text{eff}}^{\text{b})}(N)/(2E)$. Moreover, the continuous red (low N) and green (high N) curves correspond to the approximations given in eqs. (36)-(39). The different curves have been obtained with five different values of $\omega h = 16\times 4^n$, with $n = 1\ldots 5$.

3.2 Random distribution of breaks in a bundle of non-interacting fibers

As another interesting limiting case, we consider here a bundle system composed of M non-interacting fibers, subject to the effect of N randomly distributed breaks. We suppose that all fibers have the same Young modulus E, and that the breaks are distributed with the uniform probability $1/M$ among the fibers. Since elastic and viscous interactions are now absent, the position of the breaks in the whole interval $(0, l)$ is not relevant: when a fiber is broken (at one or more sites) its contribution to the effective stiffness becomes zero. We approach the problem by defining an appropriate probabilistic experiment. The corresponding probability space is composed of a sequence of N numbers belonging to the set $\{1,\ldots,M\}$. In fact, the sequence represents the ordered series of breaks distributed on the fibers: $a_1,\ldots,a_N$ with $a_i\in\{1,\ldots,M\}$, *i.e.* the i-th break is located on the a_i-th fiber. The probability of the simple event identified by the ordered sequence $a_1,\ldots,a_N$ is given by

$$\Pr\{a_1,\ldots,a_N\} = \frac{1}{M^N}\,, \tag{40}$$

because of the statistical independence of the successive generations of breaks within the bundle.

We are now interested in the probability of the following event: to have n_1 breaks on the first fiber, n_2 breaks on the second one, and so forth. The question may be formulated in this alternative way: how many sequences $a_1,\ldots,a_N$ yield a distribution of breaks identified by $n_1,\ldots,n_M$ (with $\sum_{i=1}^M n_i = N$)? This number is given by $N!/(n_1!\cdot\ldots\cdot n_M!)$ and it corresponds to the classical multinomial distribution. Therefore, we have

$$\Pr\{n_1,\ldots,n_M\} = \frac{N!}{n_1!\cdot\ldots\cdot n_M!}\frac{1}{M^N}\,. \tag{41}$$

To continue our analysis, we determine the probability $\mathcal{P}_s(N)$ to have s intact fibers after the occurrence of N total breaks. When this event is realized, among the distribution numbers $n_1,\ldots,n_M$ there are s zeros and $M-s$

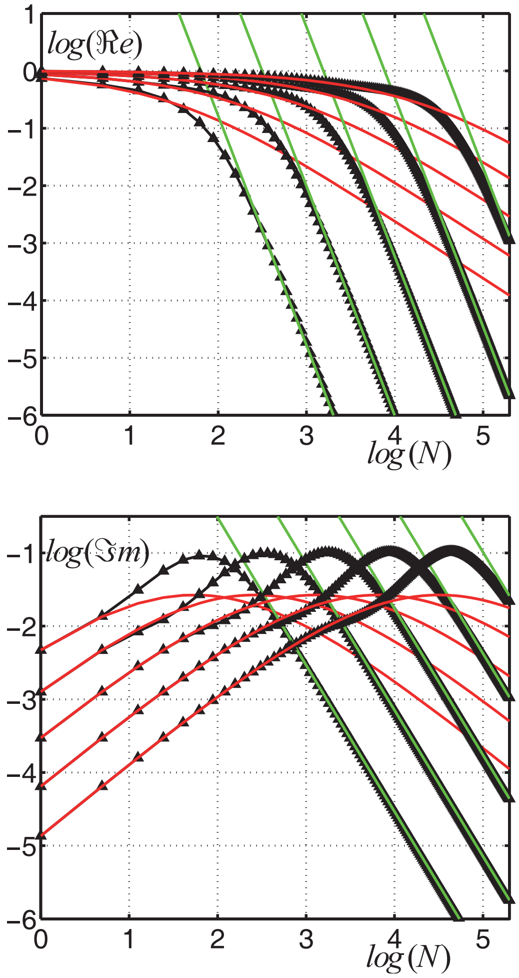

Fig. 7. Behavior of the viscous two-fiber bundle: effective stiffness (real and imaginary parts) *versus* the number of breaks in bi-logarithmic scales. See the caption of fig. 6 for details.

strictly positive numbers. Of course, there are $\binom{M}{s}$ combinations of such s zeros within the numbers $n_1, \ldots, n_M$. Therefore, we can eventually write

$$\mathcal{P}_s(N) = \binom{M}{s} \sum_{\sum_{i=1}^{M-s} n_i = N}^{n_i > 0} \frac{N!}{n_1! \cdots n_{M-s}!} \frac{1}{M^N}. \tag{42}$$

In appendix A, we sum the previous expression, eventually obtaining the following closed-form result:

$$\mathcal{P}_s(N) = \frac{M!}{s! M^N} \mathcal{S}_N^{M-s}, \tag{43}$$

where $\mathcal{S}_n^m$ represent the Stirling number of the second kind (see details in appendix A). By using the explicit relation giving these numbers, we can write $\mathcal{P}_s(N)$ in the following form

$$\mathcal{P}_s(N) = \frac{1}{M^N} \sum_{j=0}^{M-s} (-1)^{M-s-j} \binom{M}{s} \binom{M-s}{j} j^N. \tag{44}$$

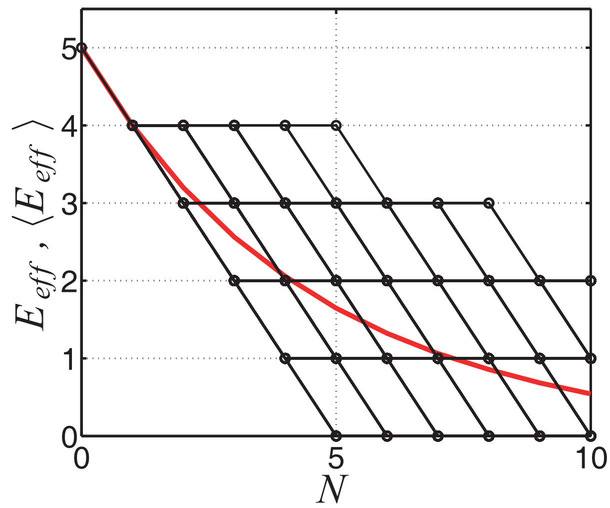

Fig. 8. Random degradation of a bundle with $M = 5$ fibers. The stochastic generation of breaks distributions (each one represented by a path in the grid) creates a tree of possibilities (the black lines correspond to E_{eff}), whereas the average value $\langle E_{\text{eff}} \rangle$ (dashed red line) corresponds to eq. (46).

In appendix B, we also prove that the probabilities $\mathcal{P}_s(N)$ ($\forall s = 0, \ldots, M$) generate a complete probability space, *i.e.*

$$\sum_{s=0}^{M} \mathcal{P}_s(N) = 1. \tag{45}$$

The most important result obtained through the $\mathcal{P}_s(N)$ concerns the average value of the Young modulus of the fiber bundle, in terms of the number of the N randomly distributed breaks. Indeed, as proved in appendix B, we can write

$$\langle E_{\text{eff}} \rangle = E \sum_{s=0}^{M} s \mathcal{P}_s(N) = ME \left(\frac{M-1}{M} \right)^N. \tag{46}$$

It is interesting to note that for large values of M we have

$$\frac{\langle E_{\text{eff}} \rangle}{ME} = e^{-N[\log(M) - \log(M-1)]} \cong e^{-N/M}. \tag{47}$$

This important result means that the mechanical degradation in a bundle of non-interacting fibers follows an exponential law. Moreover, the effective Young modulus depends only on the single variable N/M, showing a scaling behavior of the number of fibers M. As an example, in fig. 8 we consider a bundle with $M = 5$ and we show E_{eff} *versus* N for randomly chosen breaks: we note that the corresponding black lines generate a sort of tree of possibilities composed of all the paths of stiffness degradation. Moreover, the average value $\langle E_{\text{eff}} \rangle$ (red dashed line) corresponds to eq. (46). We remark that this curve perfectly matches the results obtained with the computational scheme of sect. 2.2, combined with the Monte Carlo technique.

Another important quantity describing the stochastic behavior of our system is given by the average number of breaks to cut the whole bundle. To determine this value we develop the following probabilistic argument. We search for the probability of the event $\mathcal{C}_N$, defined as follows: all fibers are broken after the generation of N breaks, while there was still an intact fiber after the generation of $N-1$ breaks. This event is the intersection of the two simpler events $\mathcal{A}_N$ and $\mathcal{B}_N$: $\mathcal{A}_N$ is the event with all fibers broken after the generation of N breaks, and $\mathcal{B}_N$ is the event with only one fiber remaining intact after the generation of $N-1$ breaks. We simply have $\Pr\{\mathcal{A}_N\} = \mathcal{P}_0(N)$ and $\Pr\{\mathcal{B}_N\} = \mathcal{P}_1(N-1)$. We use the conditional probabilities as follows:

$$\begin{aligned}\Pr\{\mathcal{C}_N\} &= \Pr\{\mathcal{A}_N \cap \mathcal{B}_N\}\\ &= \Pr\{\mathcal{A}_N \mid \mathcal{B}_N\}\Pr\{\mathcal{B}_N\}\\ &= \frac{1}{M}\mathcal{P}_1(N-1).\end{aligned} \tag{48}$$

In eq. (48) we exploited the result $\Pr\{\mathcal{A}_N \mid \mathcal{B}_N\} = 1/M$. This can be verified since the probability to have all fibers broken after N breaks, with only one fiber intact after $N-1$ breaks, corresponds to pick the last untouched fiber over the whole M-fiber bundle. By using eq. (43) we have

$$\Pr\{\mathcal{C}_N\} = \frac{M!}{M^N}\mathcal{S}_{N-1}^{M-1}. \tag{49}$$

Also in this case the quantities $\Pr\{\mathcal{C}_N\}$ represent a complete probability space with $\sum_{N=M}^{\infty}\Pr\{\mathcal{C}_N\} = 1$, as proved in Appendix C. To conclude, we can determine the average number of breaks necessary to break all the M fibers by means of the following expression:

$$\langle N\rangle = \sum_{N=M}^{\infty} N\Pr\{\mathcal{C}_N\} = M\sum_{k=1}^{M}\frac{1}{k}, \tag{50}$$

which is rigorously proved in appendix C. We can say that $\langle N\rangle$ is the geometrical percolation threshold of the M-fiber bundle (without interactions). For a large number M of fibers we can use the asymptotic formula $\sum_{k=1}^{M}\frac{1}{k} \sim \log M + \gamma$ ($\gamma = 0,5772\ldots$ being the Euler-Mascheroni constant), by obtaining

$$\langle N\rangle \cong M(\log M + \gamma) \cong M\log M. \tag{51}$$

By using this last result, we observe that the stiffness degradation described by eq. (47), when we consider $N = \langle N\rangle$, yields $\langle E_{\text{eff}}\rangle \cong E$, representing the almost complete loss of stiffness. In fact, the original effective stiffness is ME and the final one, after accumulating $\langle N\rangle$ breaks, is E, negligible with respect to ME for $M \gg 1$.

4 Numerical results and their interpretation

In this section we consider a uniform, random distribution of N breaks in a bundle of M interacting fibers, with geometries shown in fig. 9. We perform a thorough analysis of this system by means of the general computational scheme outlined in sect. 2.2. To do this, we use

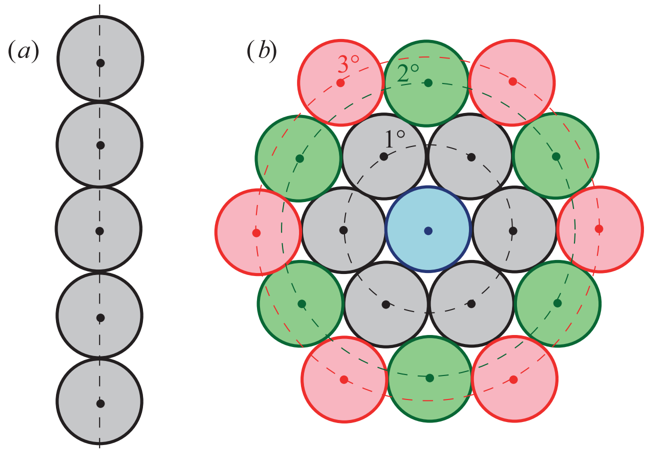

Fig. 9. Cross sectional views of bundle structures considered in our numerical investigations. In both the flat (panel a) and in the circular (panel b) bundle, we considered $7 \leq M \leq 19$. For the circular bundle, $M = 7$ corresponds to the first shell of fibers, $M = 13$ and $M = 19$ to the second and third ones, as shown in panel b.

the Monte Carlo method to generate a large number of configurations with given N and M, and to determine the resulting average values of the effective stiffness. The numerical results will be discussed and interpreted through scaling laws described by specific scaling exponents. As a final conclusion, we will prove that the overall degradation behavior can be summarized by means of the main features discussed in previous sections 3.1 and 3.2, namely: i) an exponential degradation of the effective stiffness for a low number of breaks, as observed for a bundle of non-interacting fibers (see, *e.g.* eq. (47)), and ii) a power-law like degradation for a large number of breaks, as observed for the two-fiber bundle (see, *e.g.* eq. (33)). We will therefore prove the existence of a transition between the exponential and the power-law regimes, which can be clearly explained through the underlying physical mechanisms, as discussed at length in the following.

The results have been obtained through a Monte Carlo method based on the determination of the average value over 300 realisations of each structure. For instance, it means that for considering $N = 300$ breaks within the bundle of $M = 19$ fibers we determined 300×300 matrix exponentials for 38×38 sized matrices. Moreover, we considered all values of M in the range $7 \leq M \leq 19$. The principal results of the Monte Carlo simulations are summarized in figs. 10 and 11, where the effective stiffness is represented in linear, semi- and bi-logarithmic scales. In fig. 10 the plot of the quantity $\langle E_{\text{eff}}\rangle/E$ *versus* N is parametrized by kl^2/E (with fixed $M = 19$) and, conversely, in fig. 11 the degradation curves are parametrized by M (with a fixed $kl^2/E = 0.045$). In our calculations, we considered both the aligned fiber bundle shown in fig. 9a and the circular bundle shown in fig. 9b. In both cases we used $7 \leq M \leq 19$: the minimum value $M = 7$ corresponds to a triangular lattice based bundle with one circular layer (centered hexagon), while the maximum value $M = 19$

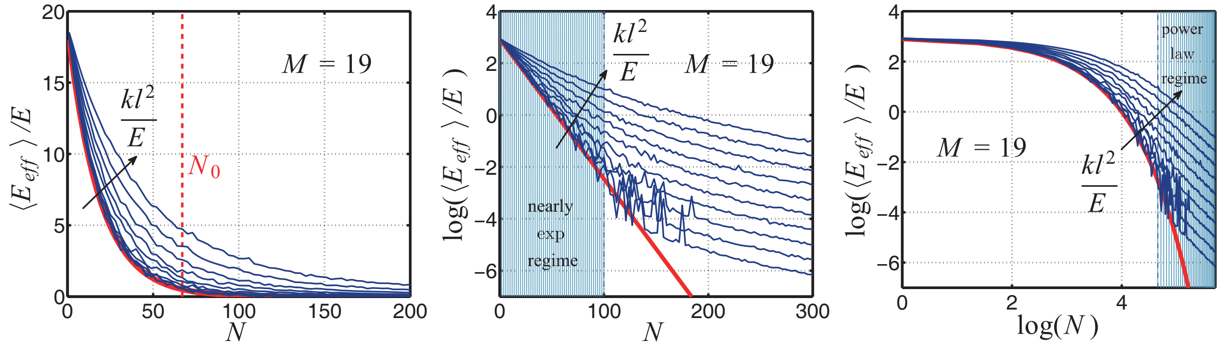

Fig. 10. Monte Carlo results for $\langle E_{\text{eff}} \rangle / E$ *versus* N in linear, semi-logarithmic and bi-logarithmic scales. We considered a bundle with $M = 19$ fibers and the following values of kl^2/E: 0.045, 0.08, 0.14, 0.25, 0.45, 0.8, 1.4, 2.5, 4.5 and 8. The red curves corresponds to $k = 0$, *i.e.* to the theory outlined in sect. 3.2. In the first panel the red dashed straight line indicates the geometrical percolation threshold $N_0 = \langle N \rangle$. The shaded areas indicate the nearly exponential and the power-law regimes.

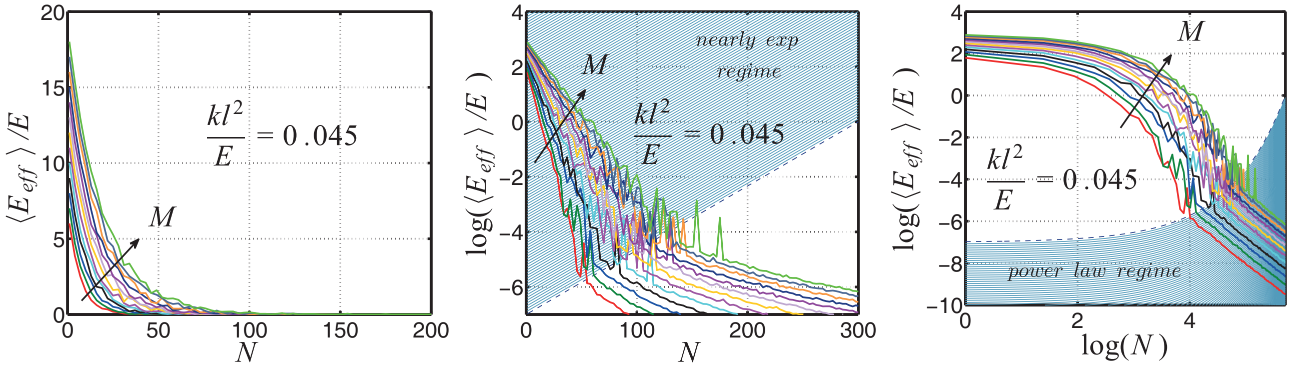

Fig. 11. Monte Carlo results for $\langle E_{\text{eff}} \rangle / E$ *versus* N in linear, semi-logarithmic and bi-logarithmic scales. We considered $kl^2/E = 0.045$ (the lowest interaction) and 13 values of M, from 7 to 19. As in fig. 10, the shaded areas indicate the nearly exponential and the power-law regimes.

represents the structure with three circular layers, as in fig. 9b. However, for sake of simplicity, in figs. 10 and 11 we report only the results for the aligned fiber bundle. Nevertheless, we underline that the curves corresponding to the circular bundle are very similar from both the qualitative and quantitative point of view.

In fig. 10 the red curves corresponds to $k = 0$ (absence of interactions), *i.e.* to eqs. (46) and (47) of sect. 3.2. In the same figure we also represented other curves (blue) corresponding to an increasing elastic interaction among the fibers. Of course, as it can be simply deduced from the first panel, a larger value of kl^2/E postpones to larger N the mechanical degradation of the bundle for a fixed number of breaks, as expected. However, contrarily to the case without interactions, we can identify two specific degradation regimes: i) for low values of N, the straight lines in the second panel of fig. 10 correspond to an nearly exponential response, while, for high values of N, the straight lines in the third panel of fig. 10 correspond to a power-law regime. These regimes have been represented by shaded areas in figs. 10 and 11, for the sake of clarity. The transition between these regimes is very sharp for low values of k and smoother for higher values. Indeed, for high intensity of the interactions the initial degradation in only approximately exponential: for this reason we named this behavior as nearly exponential regime. By observing fig. 11, we can finally conclude that the above behavior is confirmed for any number of fibers composing the bundle. It is therefore important to thoroughly analyse the scaling properties of both the nearly exponential and the power-law regimes.

Moreover, we show in fig. 10 (red dashed line) the threshold $N_0 \triangleq \langle N \rangle \cong M(\log M + \gamma)$, indicating the average number of breaks necessary to cut all fibers (geometrical percolation threshold). The corresponding stiffness without interactions decreases from ME (without breaks) to E (with $\langle N \rangle$ breaks), as thoroughly discussed after eq. (51). It is evident that N_0 is not related to the transition between the nearly exponential and the power-law regimes, defined below. The purely geometrical interpretation is therefore not sufficient and we have to search for a more physical explanation of the degradation transition.

4.1 Nearly exponential regime

We start by analysing the regime of the mechanical degradation for small values of the number of breaks N. In particular we study the initial slope of $E_{\text{eff}}(N)$ *versus* N. We already know from eq. (47) that, without interactions

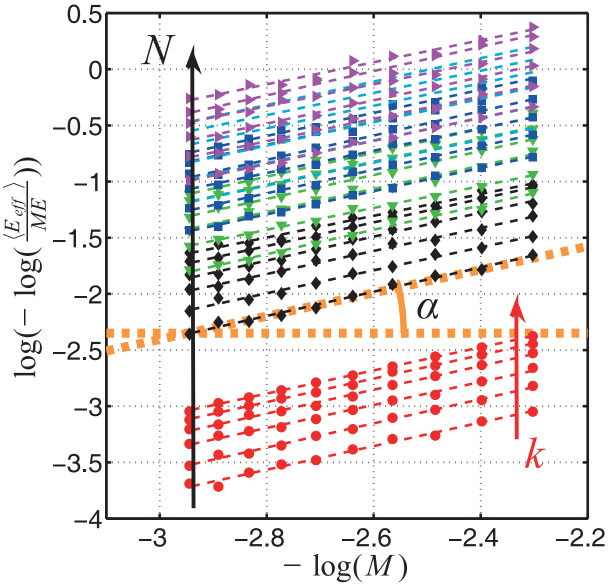

Fig. 12. Numerical determination of the parameter α through the plot of $\log[-\log\langle E_{\rm eff}\rangle/(ME)]$ *versus* $-\log(M)$ for low values of N.

Table 2. Parameters and scaling exponents characterizing the nearly exponential and the power-law regimes. All quantities are defined in eqs. (53) and (55). They correspond to a bundle with a large number M of fibers (we verified that $M \gtrsim 10$ is typically sufficient to obtain stable results).

	Aligned fiber bundle	Circular fiber bundle
α	0.97 ± 0.06	1.05 ± 0.12
a	-0.90 ± 0.05	-0.90 ± 0.07
b	2.08 ± 0.11	2.08 ± 0.21
$b\beta$	2.29 ± 0.19	2.60 ± 0.35
$b\nu$	1.97 ± 0.24	1.91 ± 0.37
β	1.09 ± 0.07	1.25 ± 0.08
ν	0.94 ± 0.08	0.92 ± 0.10

among the fibers, we should have

$$\frac{\mathrm{d}}{\mathrm{d}N}\frac{\langle E_{\rm eff}\rangle}{ME}\bigg|_{N=0} = -\frac{1}{M}\,, \tag{52}$$

in the limit of a large number M of fibers. Moreover, if we consider the fiber interactions in the bundle system, we must consider an additional variable given by $\xi = \sqrt{kl^2/E}$, as discussed in sect. 3.1 (see for instance eq. (29)). Therefore, we can presuppose a generalised slope described by the following expression

$$\frac{\mathrm{d}}{\mathrm{d}N}\frac{\langle E_{\rm eff}\rangle}{ME}\bigg|_{N=0} = -\varphi\left(\sqrt{\frac{kl^2}{E}}\right)\frac{1}{M^\alpha}\,, \tag{53}$$

where $\varphi(\xi)$ is an arbitrary function, yet to be determined, describing the effects of the fiber interactions, and α is a scaling exponent. The form of $\varphi(\xi)$ can be determined directly from the numerical results. In order to have a coherence between eq. (52) and eq. (53) for $k = 0$, it must be $\varphi(0) = 1$ and $\alpha = 1$. Below, we will numerically verify these properties. It is also important to observe that, at least for low values of k and N, we can hypothesize an exponential degradation behavior of the effective stiffness, given by

$$\log\frac{\langle E_{\rm eff}\rangle}{ME} = -\varphi\left(\sqrt{\frac{kl^2}{E}}\right)\frac{N}{M^\alpha}\,. \tag{54}$$

By using this expression we may numerically determine the exponent α by plotting $\log[-\log\langle E_{\rm eff}\rangle/(ME)]$ *versus* $-\log(M)$ for low values of N. The result is a series of straight lines with slope α, independent of N and kl^2/E, as shown in fig. 12 (for the flat bundle only, as before). The obtained numerical values of α are shown in table 2 for the flat bundle and the circular bundle. In both cases, the results are compatible with the value $\alpha = 1$, thereby proving the coherence with the achievements of sect. 3.2.

It is evident from eq. (54) that, if we plot $\langle E_{\rm eff}\rangle/(ME)$ *versus* N/M^α, we must obtain the same curve for all values of M, but different curves for different values of kl^2/E. This can be seen in the first panel of fig. 13, where we considered the lowest value of kl^2/E corresponding to 0.045. All curves for $M = 7$ to $M = 19$ are perfectly superposed, showing the peculiar scaling character of the transition between the nearly exponential and the power-law regimes. Moreover, in the second panel of fig. 13, we added the results for all values of kl^2/E. The curves are grouped for the same M, but not for the same kl^2/E, as expected.

Finally, the behavior of the system with regard to the intensity of the interactions among the fibers (modulated by kl^2/E) is controlled by the function $\varphi(\xi)$, introduced in eqs. (53) and (54). We can obtain the values of this function by plotting $-(M^\alpha/N)\log[\langle E_{\rm eff}\rangle/(ME)]$ *versus* $\sqrt{kl^2/E}$, as shown in the third panel of fig. 13 (flat and circular bundle). We proved the universal character of this function for high values of the number of fibers M. In practice, this function takes its asymptotic values already for $M \gtrsim 10$. The knowledge of this function allows the complete prediction of the system behavior for small values of N. In particular, it permits to exactly evaluate the initial slope of the curve $E_{\rm eff}$ *versus* N, as defined in eq. (53). It interesting to note that the function $\varphi(\xi)$ exhibits an asymptotic behavior for large ξ described by $\varphi(\xi) \sim c/\xi$ where $c = 1.3$ for the flat bundle and $c = 0.85$ for the circular bundle. This is useful for directly implementing the final equations, without the numerical evaluation of the function $\varphi(\xi)$, which can be simply approximated with c/ξ for large values of ξ.

The decreasing behavior of $\varphi(\xi)$ with ξ can be interpreted by observing that a large value of k (corresponding to a large value of ξ), defining a strong interaction among fibers, reduces the degradation effects induced by fractures. Indeed, small values of $\varphi(\xi)$ attenuate the right hand side of eq. (54), maintaining a larger value of effec-

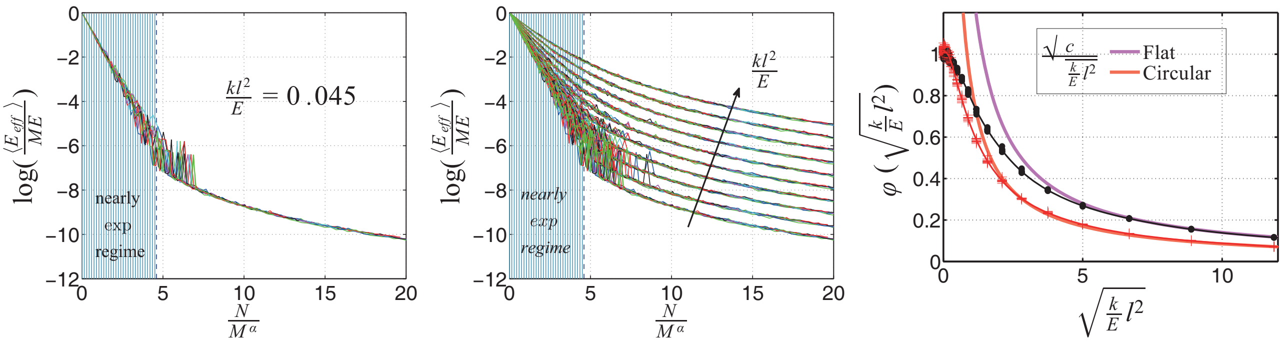

Fig. 13. First panel: Monte Carlo results for $\langle E_{\rm eff}\rangle/E$ *versus* N/M^α in semi-logarithmic scales for $kl^2/E = 0.045$. The responses for the different values of M are perfectly grouped. Second panel: as before, but including the results for the other values of kl^2/E (0.045, 0.08, 0.14, 0.25, 0.45, 0.8, 1.4, 2.5, 4.5 and 8). Now, the curves for different kl^2/E are not grouped, as expected. Third panel: numerical determination of the function $\varphi(\xi)$ defined in eq. (53). The black curve (flat bundle) and the red curve (circular bundle) are asymptotically converging to $\varphi(\xi) = c/\xi$ with $c = 1.45$ (flat bundle) and $c = 0.85$ (circular bundle).

tive stiffness. Moreover, the exponential response for low values of k and N can be also be interpreted in terms of eq. (35), obtained for a degraded dimer. As a matter of fact, eq. (35) with low values of k and N gives $E_{\rm eff}^{\rm b)}(N)/2E \simeq 1/(1+2N/z) \simeq 1-2N/z \simeq \exp(-2N/z)$, where $z = \sqrt{2}\,\xi$. The asymptotic response for the dimer is therefore given by $E_{\rm eff}^{\rm b)}(N)/2E \simeq \exp(-\varphi N/M)$ where $M = 2$ and $\varphi = 2\sqrt{2}/\sqrt{kl^2/E} = 2\sqrt{2}/\xi$. This result can be compared with eq. (54). Then, we have finally interpreted the $1/\sqrt{k}$ behavior of the argument in the exponential, coherently with the asymptotic results proved for the dimer degradation.

4.2 Power-law regime

In this subsection, we provide empirical fits, which intent to capture the underlying physics of the numerical results of Monte Carlo simulations. This can be done by using the analytical expressions, derived in sect. 3.1 above, as a guidance. In the degradation regime with a larger number of breaks, we can generalise eq. (33) through the following expression:

$$\log\frac{\langle E_{\rm eff}\rangle}{ME} = a - b\log\frac{N}{M^\beta\left(\sqrt{\frac{kl^2}{E}}\right)^\nu}, \qquad (55)$$

where the parameters a, b, β and ν must be obtained by fitting the numerical data. Equation (55) indicates that the response of the system in the regime on large N should be represented by straight lines, if we plot the quantity $\langle E_{\rm eff}\rangle/(ME)$ *versus* $N/(M^\beta\sqrt{kl^2/E}^{\,\nu})$ in bi-logarithmic scales. In order to obtain the values of the relevant parameters, we rewrite eq. (55) as follows:

$$\log\frac{\langle E_{\rm eff}\rangle}{ME} = a - b\log N + b\beta\log M + b\nu\log\sqrt{\frac{kl^2}{E}}. \qquad (56)$$

By plotting three graphs in bi-logarithmic scales of i) $\langle E_{\rm eff}\rangle/(ME)$ *versus* N, ii) $\langle E_{\rm eff}\rangle/(ME)$ *versus* M, iii) $\langle E_{\rm eff}\rangle/(ME)$ *versus* $\sqrt{kl^2/E}$, we can evaluate the slopes $-b$, $b\beta$ and $b\nu$, as well as the y-intercept a. We can therefore numerically determine all the parameters involved in eq. (55). This power-law can also be written in the form

$$\frac{\langle E_{\rm eff}\rangle}{ME} = e^a\frac{M^{b\beta}\left(\sqrt{\frac{kl^2}{E}}\right)^{b\nu}}{N^b}, \qquad (57)$$

which allows to deduct a physical explanation of the shift between the nearly exponential and the power-law regimes. With two fibers (see eq. (33)) we obtained a power-law characterized by $b = 2$, corresponding to a Young modulus decreasing as $1/N^2$. Moreover, we obtained $b\nu = 2$, a value yielding an asymptotic effective stiffness not depending on the intrinsic Young modulus E of the fibers for large N. The loss of importance of E was previously associated to the increase of importance of k, *i.e.* of the interactions between the small surviving fragments of the broken fibers. This interpretation could be extended to the general case with M fibers and N random breaks only if we numerically obtain $b\nu = 2$ (we note indeed that the symbols E appearing in the left and right hand sides of eq. (57) cancel each other out if $b\nu = 2$). The numerical results are reported in table 2 and they confirm the heuristic predictions $b = 2$, $\nu = 1$ (and, of course, $b\nu = 2$) with a good accuracy.

Furthermore, we deduce from eq. (55) that, if we plot the quantity $\langle E_{\rm eff}\rangle/(ME)$ *versus* N/M^β, we must obtain the same curve for all values of M, but different curves for different values of kl^2/E. This is in fact the result shown in the first panel of fig. 14, where we have considered the lowest value of kl^2/E corresponding to 0.045. All curves concerning the cases from $M = 7$ to $M = 19$ are perfectly superimposed, showing again the scaling character of the degradation process. In the second panel of fig. 14, we also include the results related to other values of kl^2/E. The curves are grouped with the same M, but not for the same kl^2/E, as expected. Finally, in the third panel of fig. 14, we plotted $\langle E_{\rm eff}\rangle/(ME)$ *versus* $N/(M^\beta\sqrt{kl^2/E}^{\,\nu})$ (in bi-

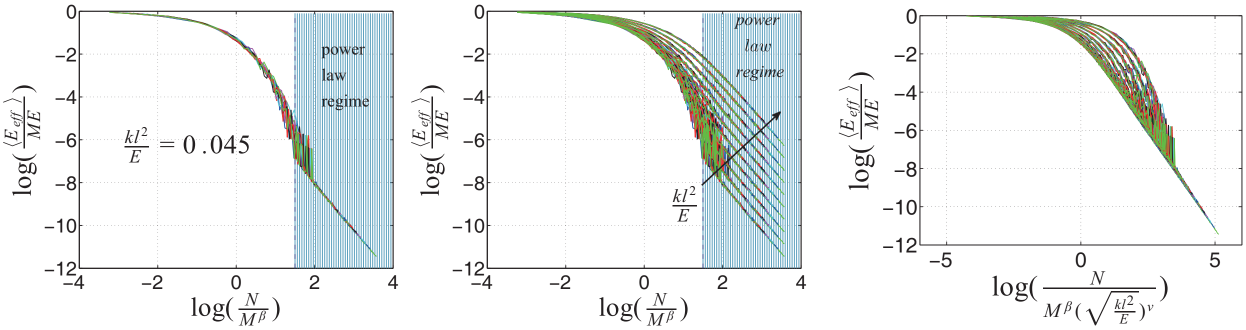

Fig. 14. First panel: Monte Carlo results for $\langle E_{\rm eff}\rangle/E$ *versus* N/M^β in bi-logarithmic scales for $kl^2/E = 0.045$. The responses for the different values of M are perfectly grouped. Second panel: as before, but including the results for the other values of kl^2/E (0.045, 0.08, 0.14, 0.25, 0.45, 0.8, 1.4, 2.5, 4.5 and 8). Now, the curves for different kl^2/E are not grouped, as expected. Third panel: plot of $\langle E_{\rm eff}\rangle/(ME)$ *versus* $N/(M^\beta \sqrt{kl^2/E}^{\,\nu})$. All curves for any M and any kl^2/E are perfectly grouped (large N).

logarithmic scale) and we show that all curves for any M and any kl^2/E are perfectly grouped: they coincide with a unique straight line, representing the universal asymptotic behavior (large N) of the bundle system.

4.3 Unifying formulation

We prove now that the nearly exponential regime and the power-law regime can be linked through a simple empirical expression, which is able to completely describe the behavior of a purely elastic bundle of M fibers with a random population of N breaks. We propose the following formulation:

$$\frac{\langle E_{\rm eff}\rangle}{ME} = \exp\left[-\varphi\left(\sqrt{\frac{kl^2}{E}}\right)\frac{N}{M^\alpha}\right] + \frac{1}{\frac{r}{N}+\eta}\,, \qquad (58)$$

where

$$\eta = \frac{e^{-a}N^b}{M^{b\beta}\left(\sqrt{\frac{kl^2}{E}}\right)^{b\nu}}\,. \qquad (59)$$

The behavior of eq. (58) corresponds to eq. (54) for low values of N, and to eq. (57) for high values of N. All parameters are therefore given in table 2 for both the flat and the circular bundle. The link between the asymptotic responses is controlled by the coefficient r, which assumes the value 1.0×10^3 for the flat bundle and the value 3.0×10^3 for the circular one. It is evident that for low value of N, the ratio r/N becomes very large, cancelling out the effects of the second term in eq. (58) and retaining the exponential term. On the other hand, for high values of N, the exponential term and the ratio r/N are negligible, resulting in $\langle E_{\rm eff}\rangle/(ME)$ to approach $1/\eta$ (see eq. (59)), as expected. The ability of eq. (58) to represent the whole behavior of the system is shown in fig. 15, where we considered the flat bundle with $M = 19$ fibers and a large spectrum of the elastic interaction parameter.

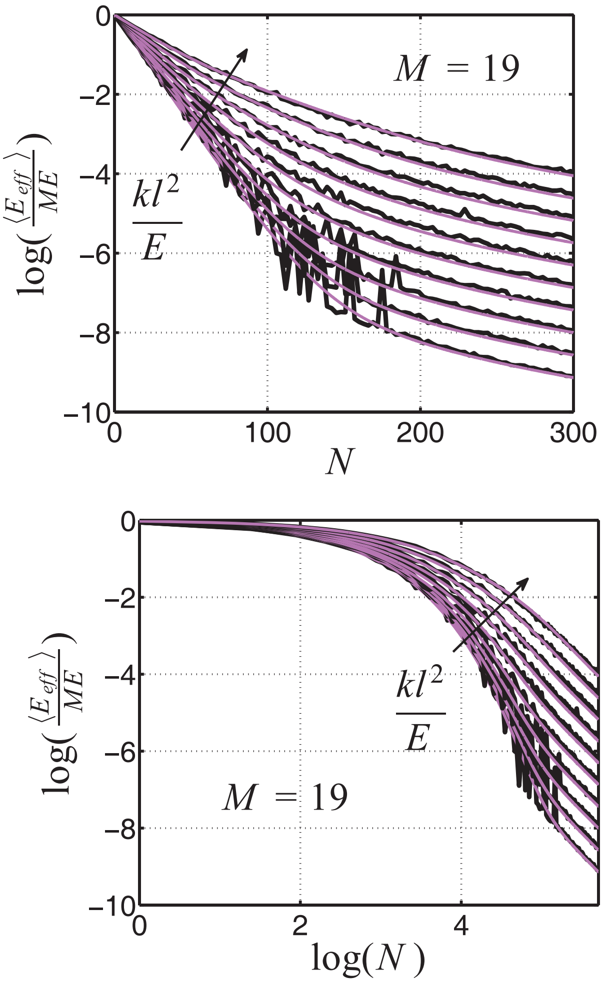

Fig. 15. Monte Carlo results (noisy black lines) and theoretical curves from eq. (58) (continuous violet lines) for $\langle E_{\rm eff}\rangle/(ME)$ *versus* N in semi-logarithmic (top panel) and bi-logarithmic (bottom panel) scales for different values of kl^2/E (0.045, 0.08, 0.14, 0.25, 0.45, 0.8, 1.4, 2.5, 4.5 and 8) and $M = 19$ (flat bundle).

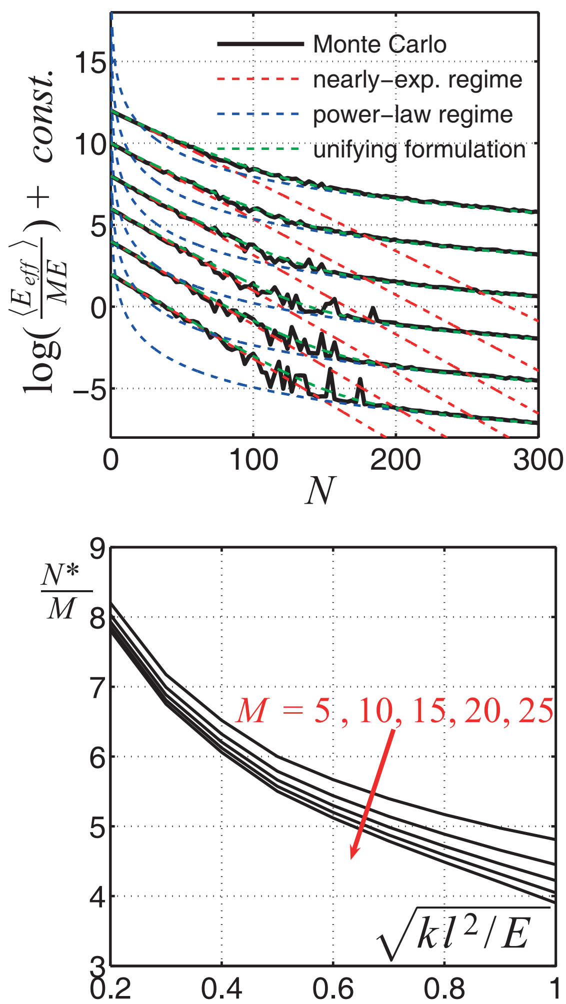

Fig. 16. Analysis of the transition point N^* between the nearly exponential and the power-law regimes. The Monte Carlo results, the asymptotic expressions and the unifying formulation have been represented for $M = 19$ (flat bundle) and for six values of $\sqrt{kl^2/E}$ (top panel). The curves have been shifted by a given constant to improve the readability. The transition location is identified by the intersection of the curves valid for low and high values of N. The final result shows N^*/M *versus* $\sqrt{kl^2/E}$ and M (bottom panel).

Since the general response is composed of two different regimes (nearly exponential and power-law), it is interesting to identify the critical value of N number of breaks corresponding to the shift between the two responses. It can be observed (see fig. 16, top panel) that this transition can be conveniently identified by the intersection point of the two asymptotic expressions, respectively valid for low and high values of N. We determined this threshold N^* for any value of M and k. From the mathematical point of view this leads to solve the following equation:

$$e^{-\varphi(\xi)\frac{N^*}{M^\alpha}} = e^a \frac{M^{b\beta}\xi^{b\nu}}{N^{*b}}, \tag{60}$$

where $\xi = \sqrt{\frac{kl^2}{E}}$. Since we can take $\alpha = 1$, $b = 2$ and $\nu = 1$, we have

$$e^{-\varphi(\xi)\frac{N^*}{M}} = e^a \frac{M^{2\beta}\xi^2}{N^{*2}}, \tag{61}$$

or, equivalently,

$$N^* = -\frac{2}{\tau}\log\frac{\sqrt{\theta}}{N^*}, \tag{62}$$

where $\tau = \varphi(\xi)/M$ and $\theta = e^a M^{2\beta}\xi^2$. In order to solve this transcendental equation we can use the following iterative scheme

$$N^*(1) = -\frac{2}{\tau}\log\sqrt{\theta}, \tag{63}$$

$$N^*(k) = -\frac{2}{\tau}\log\frac{\sqrt{\theta}}{N^*(k-1)}, \tag{64}$$

which is convergent to the exact solution. Consequently, we numerically proved that N^* is approximately proportional to M, while it depends on k through the function represented in fig. 16 for the flat bundle. Interestingly enough, we remark that N^*/M must approach infinity when $\sqrt{kl^2/E} \to 0$ since there is no transition towards the power-law regime in the absence of interactions among the fibers (for $k = 0$ we have a purely exponential degradation).

To conclude, the threshold N^* between the exponential and the power-law regimes is a decreasing function of the lateral coupling k. This slowing-down shift may have therefore practical implications since the yielding of a fiber-bundle material could be postponed by increasing the amount of lateral coupling in the bundle. Therefore, the lateral interaction among the fibers is the key ingredient in triggering this shift as a function of the crack density N.

4.4 Viscous interactions

To complete the picture of the mechanical degradation of bundles, we consider here the case of purely viscous interactions among the fibers. As before, we will perform a series of Monte Carlo simulations by considering different sizes of the bundle ($7 \le M \le 19$) and different values of the viscous coefficient h (remembering that, the quantity $i\omega h$ replaces the coefficient k of the purely elastic case). Again, we perform the analysis of both regimes, corresponding to low and high break densities. For small values of N, eq. (54) is still valid provided that we substitute k with $i\omega h$

$$\log\frac{\langle E_{\mathrm{eff}}\rangle}{ME} = -\varphi\left(\sqrt{\frac{i\omega hl^2}{E}}\right)\frac{N}{M^\alpha}. \tag{65}$$

Now, the function φ is analytically continued in order to consider complex arguments, and therefore its real and

Table 3. Parameters and scaling exponents for the purely viscous interaction among fibers. All quantities are defined in eqs. (65) and (70).

	Aligned fiber bundle	Circular fiber bundle
α	1.01 ± 0.04	1.13 ± 0.21
	Real part	
a	0.42 ± 0.07	-0.72 ± 0.12
b	4.51 ± 0.53	4.31 ± 0.58
$b\beta$	4.93 ± 0.59	5.71 ± 0.45
$b\nu$	3.98 ± 0.34	3.92 ± 0.47
β	1.09 ± 0.06	1.32 ± 0.05
ν	0.88 ± 0.09	0.91 ± 0.08
	Imaginary part	
a	-0.74 ± 0.08	-0.95 ± 0.06
b	2.11 ± 0.16	2.06 ± 0.22
$b\beta$	2.31 ± 0.23	2.66 ± 0.47
$b\nu$	1.99 ± 0.32	1.97 ± 0.31
β	1.09 ± 0.05	1.29 ± 0.07
ν	0.94 ± 0.07	0.95 ± 0.09

imaginary parts can be defined as

$$\varphi\left(\sqrt{\frac{i\omega hl^2}{E}}\right) = \varphi_R\left(\sqrt{\frac{\omega hl^2}{E}}\right) - i\varphi_I\left(\sqrt{\frac{\omega hl^2}{E}}\right). \quad (66)$$

By combining eqs. (65) and (66) the following expression is obtained:

$$\log\left(-\log\left|\frac{\langle E_{\text{eff}}\rangle}{ME}\right|\right) = \log N + \log\varphi_R\left(\sqrt{\frac{\omega hl^2}{E}}\right) - \alpha\log M, \quad (67)$$

which can be readily used to numerically determine the value of the exponent α. Indeed, if we plot the quantity $\log[-\log|\langle E_{\text{eff}}\rangle/(ME)|]$ *versus* $\log M$ (for low values of N and arbitrary values of $\omega hl^2/E$) we obtain a series of straight line having the same slope α. This value is reported in table 3 for both the flat and the circular bundles. As expected, the numerical results are compatible with the theoretical prevision $\alpha = 1$, discussed in sects. 3.2 and 4.1.

Moreover, the effects of the viscosity h among the fibers are controlled by the complex function $\varphi(\xi)$, introduced in eq. (65). We can obtain its real and imaginary parts by plotting $-(M^\alpha/N)\log[\langle E_{\text{eff}}\rangle/(ME)]$ *versus* $\sqrt{\omega hl^2/E}$, as shown in fig. 17 (for the flat and circular bundle). The knowledge of this function allows to simply evaluate the initial slope of the curve E_{eff} *versus* N, in terms of the strength of the viscous interaction. It is interesting to note that the functions $\varphi_R(\xi)$ and $\varphi_I(\xi)$ exhibit the same asymptotic behavior for large ξ described by $\varphi_{R,I}(\xi) \sim d/\xi$ where $d = 1.05$ for the flat bundle and $d = 0.65$ for the circular one (see fig. 17 for details). We conclude that the small N regime can be summed up by

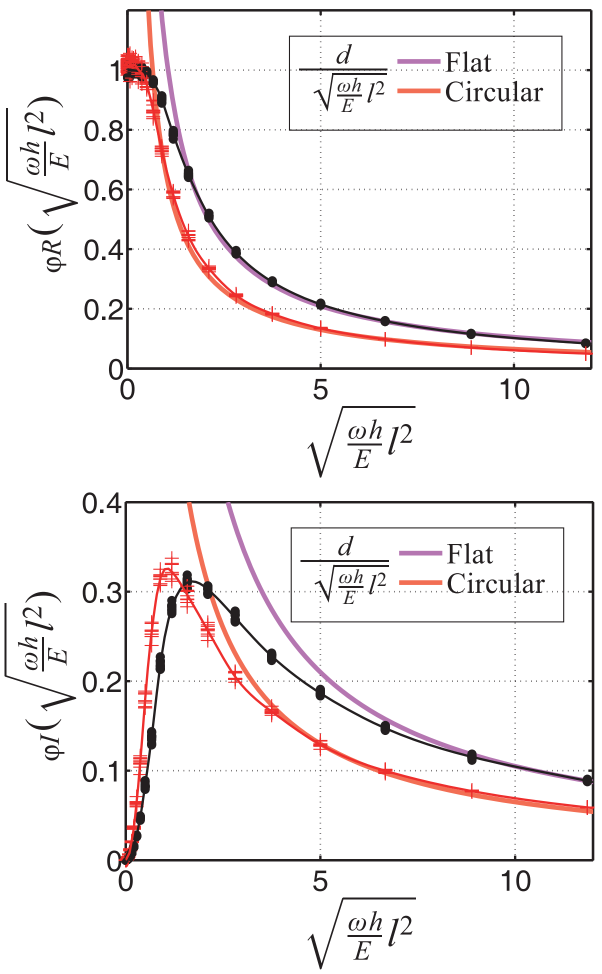

Fig. 17. Numerical determination of the functions φ_R and φ_I defined in eq. (66) as real and imaginary parts of φ. The black curves (flat bundle) and the red curves (circular bundle) are asymptotically converging to $\varphi_{R,I}(\xi) = d/\xi$ with $d = 1.05$ (flat bundle) and $d = 0.65$ (circular bundle).

the following real and imaginary parts of the effective stiffness:

$$\mathfrak{Re}\left\{\frac{\langle E_{\text{eff}}\rangle}{ME}\right\} = \exp\left(-\varphi_R\frac{N}{M^\alpha}\right)\cos\left(\varphi_I\frac{N}{M^\alpha}\right) \simeq 1 - \frac{\varphi_R N}{M^\alpha} + \left(\varphi_R^2 - \varphi_I^2\right)\frac{N^2}{2M^{2\alpha}}, \quad (68)$$

$$\mathfrak{Im}\left\{\frac{\langle E_{\text{eff}}\rangle}{ME}\right\} = \exp\left(-\varphi_R\frac{N}{M^\alpha}\right)\sin\left(\varphi_I\frac{N}{M^\alpha}\right) \simeq \frac{\varphi_I N}{M^\alpha} - \varphi_R\varphi_I\frac{N^2}{M^{2\alpha}}, \quad (69)$$

where φ_R and φ_I are implicitly considered with the argument $\sqrt{\omega hl^2/E}$.

As regards the power-law regime (large N), in this purely viscous case, we could expect a behavior similar to that observed in sect. 3.1.1 for a two-fiber bundle. Therefore, we can guess a general power-law of the form given

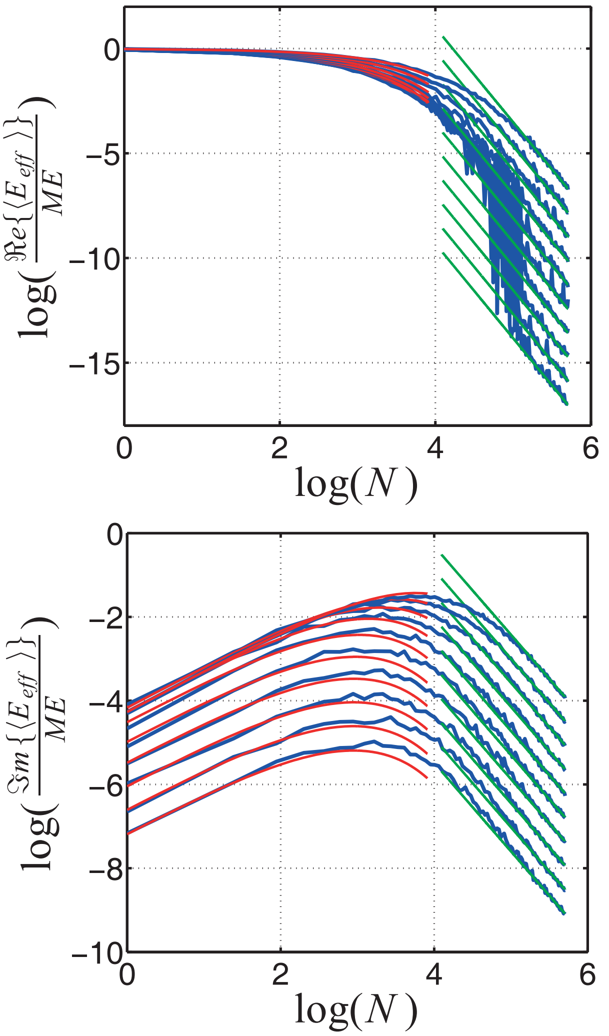

Fig. 18. Monte Carlo results (noisy black lines) and theoretical ones given in eqs. (68) and (69) (continuous red lines lines, nearly exponential regime) and in eq. (70) (continuous green lines, power-law regime) for the complex $\langle E_{\rm eff}\rangle/(ME)$ *versus* N in bi-logarithmic scales for different values of $\omega h l^2/E$ (0.045, 0.08, 0.14, 0.25, 0.45, 0.8, 1.4, 2.5, 4.5 and 8) and $M = 19$ (flat bundle).

in eq. (57)

$$\mathfrak{Re},\mathfrak{Im}\left\{\frac{\langle E_{\rm eff}\rangle}{ME}\right\} = e^a \frac{M^{b\beta}\left(\sqrt{\frac{\omega h l^2}{E}}\right)^{b\nu}}{N^b}, \qquad (70)$$

where the parameters for the real and imaginary parts may be different. For instance, for the two-fiber bundle we analytically obtain $b = 4$ for the real part and $b = 2$ for the imaginary one. By means of the procedure outlined in sect. 4.2 we numerically obtained all parameters (reported in table 3), which are fully compatible with the interpretation given in sect. 3.1.1.

In fig. 18 we show the Monte Carlo results for fiber bundles with purely viscous interactions, together with the asymptotic representations given in eqs. (68) and (69) (nearly exponential regime, red curves) and in eq. (70) (power-law regime, green straight lines). It is interesting to observe that the imaginary part of the effective stiffness of the degraded bundle shows a maximum in correspondence to a given number of breaks, as already observed in sect. 3.1.1. This can be explained as follows. To begin, we recognize that the stiffness is certainly real (being equal to ME) for $N = 0$. Moreover, an early state of degradation allows the fiber fragments to move with respect to the others, by experiencing the viscous interactions thus generating a complex valued effective stiffness. While its real part decreases with N (degradation), the imaginary part must increase. On the other hand, when the degradation is larger, both the real and imaginary part must decrease to zero, by following the above discussed power-laws. We finally observe in fig. 18 the good agreement between the limiting behaviors (small N and large N) and the numerical Monte Carlo results (similar results, not explicitly shown here, have been obtained also for the circular bundle).

5 Conclusions

The fiber bundle assembly is a system largely investigated to better understand the failure phenomena in structured materials. For the technologically important problem of a structural degradation generated by external non-mechanical agents, such as chemicals or radiations, no theoretical descriptions have been developed up to now. The well-studied fiber bundle model in fact can only deal with a degradation induced by an applied mechanical stress. Therefore, in this work we developed a theoretical and numerical scheme to analyse the mechanical properties of a bundle structure degraded by a random population of breaks distributed within the ensemble of interacting fibers. Our model is able to include elastic, viscous and visco-elastic response for the fibers and for their interactions. Although the progressive damage originated by the load redistribution is a relevant effect, widely studied through the fiber bundle model, it was not included here in order to better isolate the statistical behavior induced by the random populations of breaks. Therefore, our problem belongs to the class of homogenization theories: it concerns the determination of the effective mechanical properties of a fully interacting fiber bundle with a given distribution of breaks. We suppose that a single breaks represents a cut of a fiber (with the total interruption of the transmission of forces), which however does not affect the matrix where the fibers are embedded.

The proposed theory shows a very peculiar feature, the degradation behavior being composed of two regimes: a first exponential degradation at small number of breaks and a second power-law scaling at increasing number of breaks. The shift (or transition) between these two regimes is governed by a threshold number of breaks, which is a decreasing function of the lateral coupling. Therefore, the degradation behavior could be delayed, by increasing the lateral coupling (*i.e.* anticipating the shift to small concentrations of defects). In this respect, we predict the existence of an unprecedented exponential to power-law slowing-down shift in the degradation of a multi-cracked bundle. The physical origin of this transition between exponential and power-law degradation regimes can be summed up as follows. For a small number of cracks the overall elasticity is governed by the Young modulus of fibers, which can experience a sensible deformation since they are not strongly degraded. Moreover, in this regime the shear coupling is less important since all fibers deform almost identically. On the other hand, when the bundle is extremely degraded, fibers are composed of a large number of very short segments. Hence, segments do not undergo a considerable deformation and the overall elasticity is originated by the shear effect among them. Finally, in this second regime, the most important parameter is the interaction constant k, which modulate the complex shear phenomena. Concerning possible perspectives dealing with these shear effects, we can mention the analysis of the effective behavior of heterogeneous bundles, where the Young modulus of each fiber is a varying function of the longitudinal coordinate. In this situation, the shear phenomena are present also in the case of an intact bundle and they could be at the origin of the improved effective elastic response of several biological structures. Therefore, the disorder arising in many natural bundles can be beneficial for the elastic behavior. A further analysis could concern the effects of a population of breaks in heterogeneous or composite bundles.

The proposed model can be applied to many real situations as discussed in the Introduction. Notably, in radiation (by ionizing beams) or chemical (by enzymatic digestion) damage of DNA bundles, the knowledge of the degradation dynamics is very useful to properly design therapy protocols. In related experiments [65–68], a bundle of DNA chains is trapped between the arms of a silicon nano-tweezers, the external agent is applied and the mechanical characteristics of the trapped bundle are measured in real time. An exponential degradation has been consistently measured in such experiments, which exactly corresponds to the first regime found in our investigation. Moreover, a strong dependence on the viscosity of the solution has been observed for the degradation rate of the mechanical response. Although no quantitative results are yet available from these experiments [80], there are indications that larger values of the viscosity in strongly degraded DNA bundles lead to a complex dynamics, which might correspond to the predicted scaling shift.

We acknowledge the partial financial support by the projects "TWEEZ-RT", Mechanical Nanotweezers and Microfluidic Setup for the Direct Assay of DNA Damage by Therapeutic Radiation Beams (INSERM - Plan Cancer 2009-2013) and "MODCEL", Computer modelling of cell proliferation and damage, from senescence to radiation therapy (SIRIC, ONCOLille 2014). Computer resources provided in part by GENCI/CINES under project 097222 (2014). We also thank the Referee for his useful suggestions.

Appendix A. Determination of probabilities $\mathcal{P}_s(N)$

To find the exact expression for the probabilities $\mathcal{P}_s(N)$ we consider eq. (42), where the numbers $n_1, \ldots, n_{M-s}$ must be strictly positive to guarantee $M-s$ broken fibers. Hence, we can define $j_i = n_i - 1$ and we rewrite eq. (42) as follows:

$$\mathcal{P}_s(N) = \binom{M}{s} \sum \frac{N!}{(j_1+1)! \cdots (j_{M-s}+1)!} \frac{1}{M^N}, \tag{A.1}$$

where the sum must be performed over all the integers j_i such that $\sum_{i=1}^{M-s} j_i = N-M+s$ and $j_i \geq 0$. To approach the evaluation of this sum, we remember that the multinomial coefficients are useful to develop an arbitrary power of a polynomial, as follows:

$$(x_1 + \ldots + x_r)^n = \sum_{\sum_{i=1}^r n_i = n}^{n_i \geq 0} \frac{N!}{n_1! \cdots n_r!} x_1^{n_1} \cdots x_r^{n_r}. \tag{A.2}$$

From eq. (A.2) we easily obtain by integration

$$\begin{aligned} \mathcal{I}_n^r &\triangleq \int_0^1 \cdots \int_0^1 (x_1 + \ldots + x_r)^n \mathrm{d}x_1 \cdots \mathrm{d}x_r \\ &= \sum_{\sum_{i=1}^r n_i = n}^{n_i \geq 0} \frac{N!}{(n_1+1)! \cdots (n_r+1)!}. \end{aligned} \tag{A.3}$$

Thus, by combining eq. (A.1) with eq. (A.3) we obtain an expression for the probabilities $\mathcal{P}_s(N)$

$$\mathcal{P}_s(N) = \binom{M}{s} \frac{N!}{M^N (N-M+s)!} \mathcal{I}_{N-M+s}^{M-s}, \tag{A.4}$$

in terms of the integrals $\mathcal{I}_n^r$. We can now study these integrals by searching for a recursive expression useful to determine all the $\mathcal{I}_n^r$. First of all, we observe that $\mathcal{I}_n^1 = 1/(n+1)$, as we can easily verify by a direct calculation. Then, we perform the integration over x_r (*i.e.* the last variable) in $\mathcal{I}_n^r$, by obtaining

$$\begin{aligned} \mathcal{I}_n^r &= \int_{[0,1]^r} (x_1 + \ldots + x_r)^n \mathrm{d}x_1 \cdots \mathrm{d}x_r \\ &= \frac{1}{n+1} \int_{[0,1]^{r-1}} (x_1 + \ldots + x_{r-1} + 1)^{n+1} \mathrm{d}x_1 \cdots \mathrm{d}x_{r-1} \\ &\quad - \frac{1}{n+1} \int_{[0,1]^{r-1}} (x_1 + \ldots + x_{r-1})^{n+1} \mathrm{d}x_1 \cdots \mathrm{d}x_{r-1} \\ &= \frac{1}{n+1} \int_{[0,1]^{r-1}} \left\{ \sum_{k=0}^{n+1} \binom{n+1}{k} (x_1 + \ldots + x_{r-1})^k \right\} \\ &\quad \times \mathrm{d}x_1 \cdots \mathrm{d}x_{r-1} - \frac{1}{n+1} \mathcal{I}_{n+1}^{r-1} \\ &= \frac{1}{n+1} \sum_{k=0}^{n+1} \binom{n+1}{k} \mathcal{I}_k^{r-1} - \frac{1}{n+1} \mathcal{I}_{n+1}^{r-1} \\ &= \frac{1}{n+1} \sum_{k=0}^{n} \binom{n+1}{k} \mathcal{I}_k^{r-1} \end{aligned} \tag{A.5}$$

and, hence

$$\mathcal{I}_n^r = \frac{1}{n+1} \sum_{k=0}^{n} \binom{n+1}{k} \mathcal{I}_k^{r-1}, \tag{A.6}$$

with the initial condition $\mathcal{I}_n^1 = 1/(n+1)$. Through this iterative solution we can now determine all the integrals $\mathcal{I}_n^r$. However, we can also obtain a direct relationship between $\mathcal{I}_n^r$ and the Stirling numbers of the second kind $\mathcal{S}_n^r$ [81,82]. More specifically, we can prove that

$$\mathcal{I}_n^r = \frac{n!r!}{(n+r)!}\mathcal{S}_{n+r}^r = \mathcal{B}(n+1,r+1)\mathcal{S}_{n+r}^r, \tag{A.7}$$

where $\mathcal{B}(x,y)$ represents the Euler Beta function [82]. In fact, the recursive formula in eq. (A.6) rewritten in terms of $\mathcal{S}_n^r$ (by using eq. (A.7)) reads

$$\mathcal{S}_{q+1}^{m+1} = \frac{1}{m+1}\sum_{k=m}^{q}\binom{q+1}{k}\mathcal{S}_k^m, \tag{A.8}$$

which is exactly one recurrence equation for the Stirling numbers of the second kind, as reported in the Abramovitz-Stegun handbook [81] (to prove this statement it is sufficient to use $r=1$ in the second relationship at page 825). We remark that, incidentally, eq. (A.7) represents the finite expression of the multiple integrals defined in eq. (A.3) in terms of the Stirling numbers or, conversely, an interesting integral form of the Stirling numbers themselves. The Stirling numbers of the second kind $\mathcal{S}_n^m$ represent the number of ways of partitioning a set of n elements into m non-empty subsets [81,82]. Their closed form is [81,82]

$$\mathcal{S}_n^m = \frac{1}{m!}\sum_{k=0}^{m}(-1)^{m-k}\binom{m}{k}k^n. \tag{A.9}$$

By using eqs. (A.4), (A.7) and (A.9) we finally prove eqs. (43) and (44) of the main text.

Appendix B. Proof that $\sum_{s=0}^{M}\mathcal{P}_s(N)=1$ and $\sum_{s=0}^{M}s\mathcal{P}_s(N)=(M-1)^N/M^{(N-1)}$

We verify that, for a fixed number N of breaks, the probabilities $\mathcal{P}_s(N)$ generate a complete probability space. To begin this proof we observe that

$$\sum_{s=0}^{M}\mathcal{P}_s(N) = \frac{M!}{M^N}\sum_{s=0}^{M}\frac{\mathcal{S}_N^{M-s}}{s!} = \frac{M!}{M^N}\sum_{k=0}^{M}\frac{\mathcal{S}_N^k}{(M-k)!}. \tag{B.1}$$

Now we sum the expression $\sum_{k=0}^{M}\frac{\mathcal{S}_N^k}{(M-k)!}$ by means of the following generating function for the Stirling numbers of the second kind [81,82]

$$\frac{(e^x-1)^k}{k!} = \sum_{n=0}^{+\infty}\mathcal{S}_n^k\frac{x^n}{n!}. \tag{B.2}$$

We can multiply both sides by $M!/(M-k)!$

$$\frac{M!}{k!(M-k)!}(e^x-1)^k = \sum_{n=0}^{+\infty}\frac{M!}{(M-k)!}\mathcal{S}_n^k\frac{x^n}{n!}, \tag{B.3}$$

and then we can sum over k, as follows:

$$\sum_{k=0}^{M}\binom{M}{k}(e^x-1)^k = \sum_{n=0}^{+\infty}\sum_{k=0}^{M}\frac{M!}{(M-k)!}\mathcal{S}_n^k\frac{x^n}{n!}, \tag{B.4}$$

or, equivalently

$$e^{Mx} = \sum_{n=0}^{+\infty}\left(\sum_{k=0}^{M}\frac{M!}{(M-k)!}\mathcal{S}_n^k\right)\frac{x^n}{n!}. \tag{B.5}$$

Recalling the standard exponential power series $e^{Mx} = \sum_{n=0}^{+\infty}M^n x^n/n!$, we obtain by comparison

$$\sum_{k=0}^{M}\frac{\mathcal{S}_N^k}{(M-k)!} = \frac{M^n}{M!}. \tag{B.6}$$

Finally, by combining eq. (B.1) with eq. (B.6), we prove that $\sum_{s=0}^{M}\mathcal{P}_s(N)=1$, as requested.

To conclude, we also determine the value of the sum $\sum_{s=0}^{M}s\mathcal{P}_s(N)$, useful to study the effective Young modulus of the degraded bundle without interactions. We preliminary observe that

$$\begin{aligned}\sum_{s=0}^{M}s\mathcal{P}_s(N) &= \frac{M!}{M^N}\sum_{s=1}^{M}\frac{\mathcal{S}_N^{M-s}}{(s-1)!}\\ &= \frac{M!}{M^N}\sum_{k=0}^{M-1}\frac{\mathcal{S}_N^k}{(M-k-1)!}.\end{aligned} \tag{B.7}$$

We use again eq. (B.6) with M substituted by $M-1$ obtaining

$$\sum_{s=0}^{M}s\mathcal{P}_s(N) = \frac{(M-1)^N}{M^{(N-1)}}. \tag{B.8}$$

This final relation directly proves eq. (46) of the main text.

Appendix C. Proof that $\sum_{N=M}^{+\infty}\Pr\{\mathcal{C}_N\}=1$ and $\sum_{N=M}^{+\infty}N\Pr\{\mathcal{C}_N\}=M\sum_{k=1}^{M}1/k$

We begin by proving that the quantities $\Pr\{\mathcal{C}_N\}$ (for $N=M,\dots,+\infty$) represent a complete probability space with $\sum_{N=M}^{+\infty}\Pr\{\mathcal{C}_N\}=1$. First of all, by using eq. (49), we can elaborate the sum in this way

$$\begin{aligned}\sum_{N=M}^{+\infty}\Pr\{\mathcal{C}_N\} &= (M-1)!\sum_{N=M}^{+\infty}\frac{\mathcal{S}_{N-1}^{M-1}}{M^{N-1}}\\ &= (M-1)!\sum_{k=M-1}^{+\infty}\frac{\mathcal{S}_k^{M-1}}{M^k}.\end{aligned} \tag{C.1}$$

We try now to evaluate the last sum in eq. (C.1). To do this we use another generating function of the Stirling numbers of the second kind [81,82]

$$\frac{1}{1-x}\cdot\frac{1}{1-2x}\cdot\ldots\cdot\frac{1}{1-Mx} = \sum_{N=M}^{+\infty}\mathcal{S}_N^M x^{N-M}, \tag{C.2}$$

which is convergent for $|x|<1/M$. If we use eq. (C.2) with $x=1/(M+1)$ we obtain

$$\prod_{\alpha=1}^{M}\frac{M+1}{M+1-\alpha} = \sum_{N=M}^{+\infty}\mathcal{S}_N^M\frac{(M+1)^M}{(M+1)^N}, \tag{C.3}$$

or, after some straightforward calculation

$$\sum_{N=M}^{+\infty}\frac{\mathcal{S}_N^M}{(M+1)^N} = \frac{1}{M!}. \tag{C.4}$$

If we substitute M with $M-1$ in previous eq. (C.4) we exactly obtain the sum needed in eq. (C.1), eventually proving that $\sum_{N=M}^{+\infty} \Pr\{\mathcal{C}_N\} = 1$.

We consider now the sum $\sum_{N=M}^{+\infty} N \Pr\{\mathcal{C}_N\}$ corresponding to the average value of breaks necessary to cut the whole bundle. It can be written as follows:

$$\sum_{N=M}^{+\infty} N \Pr\{\mathcal{C}_N\} = \sum_{N=M}^{+\infty} \frac{NM!}{M^N} \mathcal{S}_{N-1}^{M-1}$$
$$= (M-1)! \sum_{k=M-1}^{+\infty} \frac{k+1}{M^k} \mathcal{S}_k^{M-1}. \quad \text{(C.5)}$$

To sum this expression we perform the derivative of eq. (C.2) with respect to the variable x

$$\frac{\mathrm{d}}{\mathrm{d}x} \prod_{\alpha=1}^{M} \frac{1}{1-\alpha x} = \sum_{N=M}^{+\infty} (N-M) \mathcal{S}_N^M x^{N-M-1}. \quad \text{(C.6)}$$

The right hand side can be elaborated as follows:

$$\frac{\mathrm{d}}{\mathrm{d}x} \prod_{\alpha=1}^{M} \frac{1}{1-\alpha x} = \sum_{N=M}^{+\infty} (N+1) \mathcal{S}_N^M x^{N-M-1}$$
$$- \sum_{N=M}^{+\infty} (M+1) \mathcal{S}_N^M x^{N-M-1}, \quad \text{(C.7)}$$

where the second sum can be easily evaluated through the original generating function given in eq. (C.2), yielding

$$\left(\frac{\mathrm{d}}{\mathrm{d}x} + \frac{M+1}{x}\right) \prod_{\alpha=1}^{M} \frac{1}{1-\alpha x} = \sum_{N=M}^{+\infty} \frac{N+1}{x^{M+1}} \mathcal{S}_N^M x^N. \quad \text{(C.8)}$$

Now, as before, we calculate this expression for $x = 1/(M+1)$; for convenience, we define $a_\alpha = 1/(1-\alpha x)$ and we obtain

$$\frac{\mathrm{d}}{\mathrm{d}x} \prod_{\alpha=1}^{M} a_\alpha = \left(\sum_{i=1}^{M} \frac{1}{a_i} \frac{\mathrm{d}a_i}{\mathrm{d}x}\right) \prod_{\alpha=1}^{M} a_\alpha, \quad \text{(C.9)}$$
$$\prod_{\alpha=1}^{M} a_\alpha = \frac{(M+1)^M}{M!}, \quad \text{(C.10)}$$
$$\sum_{i=1}^{M} \frac{1}{a_i} \frac{\mathrm{d}a_i}{\mathrm{d}x} = \sum_{i=1}^{M} \frac{i(M+1)}{M+1-i}$$
$$= (M+1) \sum_{i=1}^{M} \left(\frac{(M+1)}{M+1-i} - 1\right)$$
$$= (M+1)\left[(M+1)H_M - M\right], \quad \text{(C.11)}$$

where $H_M = 1 + \frac{1}{2} + \frac{1}{3} + \ldots + \frac{1}{M}$ are the so-called harmonic numbers. Summing up, we can use the intermediate results in eqs. (C.9), (C.10) and (C.11) to further develop eq. (C.8) calculated for $x = 1/(M+1)$, finally obtaining

$$\sum_{N=M}^{+\infty} \frac{N+1}{(M+1)^N} \mathcal{S}_N^M = \frac{M+1}{M!} H_{M+1}. \quad \text{(C.12)}$$

The previous equation, evaluated with $M-1$ in place of M, when substituted in eq. (C.5) yields $\sum_{N=M}^{+\infty} N \Pr\{\mathcal{C}_N\} = M \sum_{k=1}^{M} 1/k$, or equivalently, eq. (50) as requested.

References

1. S.M. Rafelsky, J.A. Theriot, Annu. Rev. Biochem. **73**, 209 (2004).
2. B.L. Smith, T.E. Schaffer, M. Viani, J.B. Thompson, N.A. Frederick, J. Kindt, A. Belcher, G.D. Stucky, D.E. Morse, P.K. Hansma, Nature **399**, 761 (1999).
3. P. Fratzl, Curr. Opin. Colloid Interface Sci. **8**, 32 (2003).
4. A.B. Dalton, S. Collins, E. Munoz, J.M. Razal, V.H. Ebron, J.P. Ferraris, J.N. Coleman, B.G. Kim, R.H. Baughman, Nature **423**, 703 (2003).
5. T. Giesa, M. Arslan, N.M. Pugno, M.J. Buehler, Nanoletters **11**, 5038 (2011).
6. M. Buehler, Nano Today **5**, 379 (2010).
7. Y. Liu, S. Thomopoulos, C. Chen, V. Birman, M.J. Buehler, G.M. Genin, J. R. Soc. Interface **11**, 20130835 (2014).
8. N.M. Pugno, F. Bosia, T. Abdalrahman, Phys. Rev. E **85**, 011903 (2012).
9. G.M. Grason, Phys. Rev. Lett. **105**, 045502 (2010).
10. N.S. Gov, Phys. Rev. E **78**, 011916 (2008).
11. S.W. Cranford, J. R. Soc. Interface **10**, 20130148 (2013).
12. H.W. Zhu, C.L. Xu, D.H. Wu, B.Q. Wei, R. Vajtai, P.M. Ajayan, Science **296**, 884 (2002).
13. D. Wang, P. Song, C. Liu, W. Wu, S. Fan, Nanotechnology **19**, 075609 (2008).
14. K. Hata, D.N. Futaba, K. Mizuno, T. Namai, M. Yumura, S. Iijima, Science **19**, 1362 (2004).
15. L. Liu, W. Ma, Z. Zhang, Small **7**, 1504 (2011).
16. S. Kumar, T.D. Dang, F.E. Arnold, A.R. Bhattacharyya, B.G. Min, X. Zhang, R.A. Vaia, C. Park, W.W. Adams, R.H. Hauge, R.E. Smalley, S. Ramesh, P.A. Willis, Macromolecules **35**, 9039 (2002).
17. N.M. Pugno, F. Bosia, A. Carpinteri, Small **4**, 1044 (2008).
18. S. Pradhan, A. Hansen, B.K. Chakrabarti, Rev. Mod. Phys. **82**, 499 (2010).
19. H. Kawamura, T. Hatano, N. Kato, S. Biswas, B.K. Chakrabarti, Rev. Mod. Phys. **84**, 839 (2012).
20. F.T. Peirce, J. Text. Ind. **17**, T355 (1926).
21. H.E. Daniels, Proc. R. Soc. London, Ser. A **183**, 405 (1945).
22. D.G. Harlow, S.L. Phoenix, J. Compos. Mater. **12**, 195 (1978).
23. D.G. Harlow, S.L. Phoenix, J. Mech. Phys. Solids **39**, 173 (1991).
24. D. Sornette, J. Phys. A **22**, L243 (1989).
25. P.M. Duxbury, P.L. Leath, Phys. Rev. B **49**, 12676 (1994).
26. S. Zapperi, P. Ray, H.E. Stanley, A. Vespignani, Phys. Rev. Lett. **78**, 1408 (1997).
27. M. Kloster, A. Hansen, P.C. Hemmer, Phys. Rev. E **56**, 2615 (1997).
28. P. Bhattacharyya, S. Pradhan, B.K. Chakrabarti, Phys. Rev. E **67**, 046122 (2003).
29. J.B. Gómez, D. Iñiguez, A.F. Pacheco, Phys. Rev. Lett. **71**, 380 (1993).
30. A. Hansen, P.C. Hammer, Phys. Lett. A **184**, 394 (1994).
31. R.C. Hidalgo, F. Kun, H.J. Herrmann, Phys. Rev. E **65**, 032502 (2002).
32. D.C. Lagoudas, C.Y. Hui, S.L. Phoenix, Int. J. Solids Struct. **25**, 45 (1989).
33. D.D. Mason, C.Y. Hui, S.L. Phoenix, Int. J. Solids Struct. **29**, 2829 (1992).

34. I.J. Beyerlein, S.L. Phoenix, R. Raj, Int. J. Solids Struct. **35**, 3177 (1998).
35. I.J. Beyerlein, S.L. Phoenix, J. Mech. Phys. Solids **44**, 1997 (1996).
36. F. Raischel, F. Kun, H.J. Herrmann, Phys. Rev. E **73**, 066101 (2006).
37. R.C. Hidalgo, F. Kun, H.J. Herrmann, Phys. Rev. E **64**, 066122 (2001).
38. R.C. Hidalgo, F. Kun, K. Kovcs, I. Pagonabarraga, Phys. Rev. E **80**, 051108 (2009).
39. F. Kun, S. Nagy, Phys. Rev. E **77**, 016608 (2008).
40. U. Divakaran, A. Dutta, Phys. Rev. E **78**, 021118 (2008).
41. C. Roy, S. Kundu, S.S. Manna, Phys. Rev. E **87**, 062137 (2013).
42. K. Kovács, R.C. Hidalgo, I. Pagonabarraga, F. Kun, Phys. Rev. E **87**, 042816 (2013).
43. K.S. Gjerden, A. Stormo, A. Hansen, Phys. Rev. Lett. **111**, 135502 (2013).
44. L.J. Walpole, Adv. Appl. Mech. **11**, 169 (1981).
45. Z. Hashin, J. Appl. Mech. **50**, 481 (1983).
46. T. Mura, *Micromechanics of Defects in Solids* (Kluwer Academic Publishers, Dordrecht, 1991).
47. Z. Hashin, S. Shtrikman, J. Appl. Phys. **33**, 3125 (1962).
48. Z. Hashin, S. Shtrikman, J. Mech. Phys. Solids **10**, 335 (1962).
49. S. Torquato, J. Mech. Phys. Solids **45**, 1421 (1997).
50. S. Torquato, J. Mech. Phys. Solids **46**, 1411 (1998).
51. J.G. Berryman, J. Acoust. Soc. Am. **68**, 1820 (1980).
52. M. Avellaneda, Commun. Pure Appl. Math. **40**, 527 (1987).
53. R. McLaughlin, Int. J. Eng. Sci. **15**, 237 (1977).
54. S. Giordano, Eur. J. Mech. A. Solids **22**, 885 (2003).
55. J.D. Eshelby, Proc. R. Soc. A **241**, 376 (1957).
56. M. Kachanov, Appl. Mech. Rev. **45**, 305 (1992).
57. M. Kachanov, Adv. Appl. Mech. **30**, 259 (1994).
58. S. Giordano, L. Colombo, Phys. Rev. Lett. **98**, 055503 (2007).
59. S. Giordano, L. Colombo, Phys. Rev. B **77**, 054106 (2008).
60. S. Giordano, P.L. Palla, Eur. Phys. J. B **85**, 59 (2012).
61. S. Giordano, A. Mattoni, L. Colombo, Rev. Comput. Chem. **27**, 1 (2011).
62. Y. Kashida, M. Kato, Antimicrob. Agents Chemother. **41**, 2389 (1997).
63. P. Cao, J.-i. Hanai, P. Tanksale, S. Imamura, V.P. Sukhatme, S.H. Lecker, FASEB J. **23**, 2844 (2009).
64. J.F. Ward, Int. J. Radiat. Biol. **57**, 1141 (1990).
65. G. Perret, P.-T. Chiang, T. Lacornerie, M. Kumemura, N. Lafitte, H. Guillou, L. Jalabert, E. Lartigau, T. Fujii, F. Cleri, H. Fujita, D. Collard, in *Engineering in Medicine and Biology Society (EMBC), 35th Annual International Conference, Osaka, 2013* (IEEE, New York, 2013) p. 6820.
66. F. Manca, S. Giordano, P.L. Palla, G. Perret, E. Lartigau, D. Collard, H. Fujita, F. Cleri, *European Materials Research Society Spring Meeting, E-MRS Spring 2014, Lille, Symposium N - Converging technology for nanobio-applications*.
67. M. Kumemura, D. Collard, S. Yoshizawa, D. Fourmy, N. Lafitte, S. Takeuchi, T. Fujii, L. Jalabert, H. Fujita, in *International Conference on Micro Electro Mechanical Systems (MEMS2010), Hong Kong* (IEEE, New York, 2010) p. 915.
68. M. Kumemura, D. Collard, R. Tourvielle, N. Lafitte, K. Montagne, S. Yoshizawa, D. Fourmy, C. Yamahata, L. Jalabert, Y. Sakai, S. Takeuchi, T. Fujii, H. Fujita, in *International Conference on Micro Electro Mechanical Systems (MEMS2011), Cancún* (IEEE, New York, 2011) p. 67.
69. E.S. Ibrahim, Electric Power Syst. Res. **52**, 9 (1999).
70. R. Betti, A. West, G. Vermaas, Y. Cao, J. Bridge Eng. **10**, 151 (2005).
71. J.P. Broomfield, *Corrosion of Steel in Concrete* (Taylor & Francis, New York, 2007).
72. D. Cohen, P. Lehmann, D. Or, Water Resour. Res. **45**, W10436 (2009).
73. Y. Matsushi, Y. Matsukura, Bull. Eng. Geol. Env. **65**, 449 (2006).
74. F. Manca, S. Giordano, P.L. Palla, F. Cleri, Phys. Rev. Lett. **113**, 255501 (2014).
75. F. Cleri, Sci. Model. Simul. **15**, 369 (2008).
76. F. Manca, S. Giordano, P.L. Palla, R. Zucca, F. Cleri, L. Colombo, J. Chem. Phys. **136**, 154906 (2012).
77. F. Manca, S. Giordano, P.L. Palla, F. Cleri, L. Colombo, J. Chem. Phys. **137**, 244907 (2012).
78. F. Manca, S. Giordano, P.L. Palla, F. Cleri, L. Colombo, Phys. Rev. E **87**, 032705 (2013).
79. F. Manca, S. Giordano, P.L. Palla, F. Cleri, Physica A **395**, 154 (2014).
80. D. Collard, Private communications (2014).
81. M. Abramowitz, I.A. Stegun, *Handbook of Mathematical Functions* (Dover Publication, New York, 1970).
82. F.W.J. Olver, D.W. Lozier, R.F. Boisvert, C.W. Clark, *NIST Handbook of Mathematical Functions* (National Institute of Standards and Technology and Cambridge University Press, New York, 2010).